Modeled production, oxidation, and transport processes of wetland methane emissions in temperate, boreal, and Arctic regions

Masahito Ueyama, Sara H Knox, Kyle B Delwiche, Sheel Bansal, William J Riley, Dennis Baldocchi, Takashi Hirano, Gavin Mcnicol, Karina Schafer, Lisamarie Windham-myers, et al.

Modeled production, oxidation and transport processes of wetland methane emissions in temperate, boreal, and Arctic regions

Masahito Ueyama[1], Sara H. Knox[2], Kyle B. Delwiche[3], Sheel Bansal[4], William J. Riley[5], Dennis Baldocchi[3], Takashi Hirano[6], Gavin McNicol[7], Karina Schafer[8], Lisamarie Windham-Myers[9], Benjamin Poulter[10], Robert B. Jackson[11], Kuang-Yu Chang[5], Jiquen Chen[12], Housen Chu[13], Ankur R. Desai[14], Sébastien Gogo[15], Hiroki Iwata[16], Minseok Kang[17], Ivan Mammarella[18], Matthias Peichl[19], Oliver Sonnentag[20], Eeva-Stiina Tuittila[21], Youngryel Ryu[22], Eugénie S. Euskirchen[23], Mathias Göckede[24], Adrien Jacotot[25], Mats Nilsson[26], Torsten Sachs[27]

[1] Graduate School of Agriculture, Osaka Metropolitan University, Sakai, Japan
[2] Department of Geography, The University of British Columbia, Vancouver, Canada
[3] Department of Environmental Science, Policy & Management, UC Berkeley, Berkeley, CA, USA
[4] U.S. Geological Survey, Northern Prairie Wildlife Research Center, Jamestown, ND 58401 USA
[5] Climate and Ecosystem Sciences Division, Lawrence Berkeley National Laboratory, Berkeley, CA, USA
[6] Research Faculty of Agriculture, Hokkaido University, Sapporo, Japan
[7] Department of Earth and Environmental Sciences, University of Illinois Chicago, Chicago, IL, USA
[8] Department of Earth and Env Science, Rutgers University Newark, NJ, USA
[9] Water Mission Area, U.S. Geological Survey, Menlo Park, CA, USA
[10] NASA Goddard Space Flight Center, Biospheric Sciences Laboratory, Greenbelt, MD, USA
[11] Department of Earth System Science, Stanford University, Stanford, CA, USA
[12] Department of Geography, Environment, and Spatial Sciences, Michigan State University, East Lansing, MI, USA
[13] Climate and Ecosystem Sciences Division, Lawrence Berkeley National Lab, Berkeley, CA, USA
[14] Dept of Atmospheric and Oceanic Sciences, University of Wisconsin-Madison, Madison, WI, USA
[15] ECOBIO (Écosystèmes, Biodiversité, Évolution), Université Rennes 1, CNRS, UMR 6553, 35000, Rennes, France

[16] Department of Environmental Science, Faculty of Science, Shinshu University, Matsumoto, Japan
[17] National Center for Agro Meteorology, Seoul, South Korea
[18] Institute for Atmospheric and Earth System Research/Physics, Faculty of Science, University of Helsinki, Helsinki, Finland
[19] Department of Forest Ecology and Management, Swedish University of Agricultural Sciences, 901 83 Umeå, Sweden
[20] Université de Montréal, Département de géographie, Université de Montréal, Montréal, QC H2V 0B3, Canada
[21] School of Forest Sciences, University of Eastern Finland, Joesnuu, Finland
[22] Department of Landscape Architecture and Rural Systems Engineering, Seoul National University, Seoul, South Korea
[23] University of Alaska Fairbanks, Institute of Arctic Biology, Fairbanks, AK, USA
[24] Max Planck Institute for Biogeochemistry, Department of Biogeochemical Signals, Jena, Germany
[25] INRAE, UMR 1069 SAS, 65 rue de Saint-Brieuc, 35042 Rennes, France
[26] Department of Forest Ecology and Management, Swedish University of Agricultural Sciences, 901 83 Umeå, Sweden
[27] GFZ German Research Centre for Geosciences, Telegrafenberg, 14473 Potsdam, Germany

Corresponding author: M. Ueyama, Graduate School of Agriculture, Osaka Metropolitan University, Sakai, Japan (Tel : +81-72-254-9432) (mueyama@omu.ac.jp)

ORCiD
M. Ueyama : https://orcid.org/0000-0002-4000-4888
S. Knox : https://orcid.org/0000-0003-2255-5835
K. B. Delwiche : https://orcid.org/0000-0002-5981-2500
S. Bansal : https://orcid.org/0000-0003-1233-1707
W. J. Riley : https://orcid.org/0000-0002-4615-2304
D. Baldocchi : http://orcid.org/0000-0003-3496-4919
T. Hirano : https://orcid.org/0000-0002-0325-3922

G. McNicol : https://orcid.org/0000-0002-6655-8045
K. Schafer : No ID
L. Windham-Myers : https://orcid.org/ 0000-0003-0281-9581
B. Poulter : https://orcid.org/ 0000-0002-9493-8600
R. B. Jackson : https://orcid.org/0000-0001-8846-7147
K.-Y. Chang : https://orcid.org/ 0000-0002-7859-5871
J. Chen : https://orcid.org/0000-0003-0761-9458
H. Chu : https://orcid.org/0000-0002-8131-4938
A. R. Desai : https://orcid.org/0000-0002-5226-6041
S. Gogo : https://orcid.org/0000-0002-0867-497X
H. Iwata : https://orcid.org/0000-0002-8962-8982
M. Kang : https://orcid.org/0000-0003-4901-4465
I. Mammarella : https://orcid.org/0000-0002-8516-3356
M. Peichl : https://orcid.org/0000-0002-9940-5846
O. Sonnentag : https://orcid.org/0000-0001-9333-9721
E.-S. Tuittila : https://orcid.org/0000-0001-8861-3167
Y. Ryu : https://orcid.org/0000-0001-6238-2479
E. S. Euskirchen : https://orcid.org/0000-0002-0848-4295
M. Göckede : https://orcid.org/0000-0003-2833-8401
A. Jacotot : https://orcid.org/0000-0002-0126-7597
M. Nilsson : https://orcid.org/0000-0003-3765-6399
T. Sachs : https://orcid.org/0000-0002-9959-4771

Abstract

Wetlands are the largest natural source of methane (CH_4) to the atmosphere. The eddy covariance method provides robust measurements of net ecosystem exchange of CH_4, but interpreting its spatio-temporal variations is challenging due to the co-occurrence of CH_4 production, oxidation, and transport dynamics. Here we estimate these three processes using a data-model fusion approach across 25 wetlands in temperate, boreal, and Arctic regions. Our data-constrained model – iPEACE – reasonably reproduced CH_4 emissions at 19 of the 25 sites with normalized root mean square error of 0.59, correlation coefficient of 0.82, and normalized standard deviation of 0.87. Among the three processes, CH_4 production appeared to be the most important process, followed by oxidation in explaining inter-site variations in CH_4 emissions. Based on a sensitivity analysis, CH_4 emissions were generally more sensitive to decreased water table than to increased gross primary productivity or soil temperature. For periods with leaf area index (LAI) of ≥20% of its annual peak, plant-mediated transport appeared to be the major pathway for CH_4 transport. Contributions from ebullition and diffusion were relatively high during low LAI (<20 %) periods. The lag time between CH_4 production and CH_4 emissions tended to be short in fen sites (3 ± 2 days) and long in bog sites (13 ± 10 days). Based on a principal component analysis, we found that parameters for CH_4 production, plant-mediated transport, and diffusion through water explained 77% of the variance in the parameters across the 19 sites, highlighting the importance of these parameters for predicting wetland CH_4 emissions across biomes. These processes and associated parameters for CH_4 emissions among and within the wetlands provide useful insights for interpreting observed net CH_4 fluxes, estimating sensitivities to biophysical variables, and modeling global CH_4 fluxes.

Running title: Estimating processes for wetland CH_4 emissions

Keywords: Methane emissions, Eddy covariance, Bayesian optimization, Multi-site synthesis, Methane model, Data-model fusion

1. Introduction

Wetlands are the largest natural source of methane (CH_4) – a potent greenhouse gas contributing to climate warming. Methane emissions from wetlands contribute approximately 20% of total annual CH_4 emissions (Saunois et al., 2020). Despite their importance, estimates of wetland CH_4 emissions are highly uncertain (Bohn et al., 2015; Melton et al., 2013) because direct measurements of CH_4 emissions (Delwiche et al., 2021) are far fewer than those of carbon dioxide (CO_2) fluxes (Pastorello et al., 2020). In particular, the variability in CH_4 emissions appears high across spatial and temporal scales (Knox et al., 2019; Delwiche et al., 2021). As a result of the associated uncertainties, current estimates of the global CH_4 budget contain large discrepancies between top-down and bottom-up approaches (Saunois et al., 2020; Jackson et al. 2020).

Methane emissions from wetlands also exhibit a wide range of magnitudes and responses to biophysical variables. Because CH_4 is primarily produced by anaerobic methanogens and oxidized by aerobic bacteria (Bridgham et al., 2013; Conrad 2009), water table depth (WTD) has been identified as an important thermodynamic boundary and thus potential predictor of wetland CH_4 emissions (Brown et al., 2014; Moore and Roulet, 1993; Rinne et al., 2018). Methanogens produce CH_4 using substrates both from carbon recently fixed through photosynthesis (Whiting and Chanton, 1993) and previously fixed carbon (Glaser et al., 2004; Karofeld and Tõnisson, 2014). Thus, CH_4 emissions are often correlated with plant primary production and/or soil respiration (Turetsky et al., 2014; Villa et al., 2020; Whiting and Chanton, 1993). Because temperature affects CH_4 production kinetics, soil temperature is typically correlated with CH_4 emissions (Knox et al., 2019; Yvon-Durocher et al., 2014), albeit substantial seasonal hysteresis was reported to occur in many sites, likely due to substrate-temperature driver interactions (Chang et al. 2020, 2021). In addition to production and oxidation, transport pathways are also crucial in modeling CH_4 emissions. Because CH_4 in soils is transported through plant aerenchyma, ebullition bubbles through standing water, and/or diffusion, CH_4 emissions were shown to be often correlated with leaf area index (LAI), latent heat flux, and/or barometric pressure (PA) (Kwon et al., 2017; Sturtevant et al., 2016; Tokida et al., 2005; Ueyama et al. 2020).

To better understand wetland CH_4 emissions, the eddy covariance (EC) method has been widely used at various wetlands along with measurements of other ancillary covariates such as WTD and soil temperature (Morin, 2018; Knox et al., 2019; Delwiche et al., 2021). The EC method provides quasi-continuous measurements of CH_4, CO_2, and energy exchanges between the land

surface and the atmosphere (Baldocchi, 2014). The direct measurements have been used to evaluate magnitudes of CH_4 emissions, their interannual variations, and their responses to various biophysical variables (Chang et al., 2021; Chu et al., 2014; Knox et al., 2019; Rinne et al., 2018; Yuan et al., 2022). Previous studies have identified biophysical variables such as soil and air temperature and WTD as the primary drivers for the temporal and spatial variations in CH_4 emissions (Knox et al., 2019; Turetsky et al., 2014; Yuan et al., 2022), but their importance varies substantially among wetlands and across time scales (Koebsch et al., 2015; Knox et al., 2021). Furthermore, complex interactions hinder the use of simple correlation analyses for disentangling responses of CH_4 emissions to biophysical variables, leading to large uncertainties when interpreting observations (Chang et al. 2020; Sturtevant et al., 2016; Knox et al., 2021). Recently, the FLUXNET-CH_4 database was curated for supporting synthesis of wetland CH_4 emissions using the EC methods (Knox et al., 2019; Delwiche et al., 2021) and, for example, was used to evaluate inter-site variations in CH_4 emissions (Chang et al. 2021; Knox et al., 2021, 2021; Yuan et al., 2022).

To improve the mechanistic understanding and accurate modeling of CH_4 emissions, the relative contributions of CH_4 emission pathways have been measured or estimated with various field measurements (Table 1). These measurements include chamber techniques (Korrensalo et al., 2022; Tokida et al., 2007a, b), bubble traps (Stanley et al., 2019), isotope techniques (Dorodnikov et al., 2011), and dissolved CH_4 concentrations in pore water (McNicol et al., 2017). Recently, a wavelet analysis of EC measurements examined the contribution of ebullition to total CH_4 emissions (Göckede et al., 2019; Iwata et al., 2018; Hwang et al., 2020; Richardson et al., 2022; Schaller et al., 2018). These analyses revealed that plant-mediated transport was the most important pathway for wetland CH_4 emissions (up to 98% of the total emissions), but the other two pathways were also important under environmental conditions such as flooded wetlands without emergent vegetation and shallow ponds. Many process-based models (Table 1) have also shown that CH_4 emissions occur mostly through plant-mediated transport (Castro-Morales et al., 2018; Ma et al., 2017; Peltola et al., 2018; Susiluoto et al., 2018; Wania et al., 2010), although one model found ebullition was the dominant pathway (Ito, 2019). Although previous studies conducted across relatively few wetland sites are useful for understanding CH_4 transport pathways, comparisons of transport mechanisms across multiple wetlands remain challenging. The challenge lies in uncertainties in measurement techniques, spatial representation of measured processes in

the field, and different model structures in process-based models.

Data-model fusion approaches have recently been used for evaluating wetland CH_4 emissions (Ma et al., 2017; Müller et al., 2015; Salmon et al., 2022; Susiluoto et al., 2018; Ueyama et al., 2022). These methods use observed data for constraining process-based models that are often difficult to calibrate, and can be used to evaluate processes of CH_4 emissions and their sensitivity to biophysical drivers. To reduce the uncertainties in a process-based model, Müller et al. (2015) used observed data for constraining a model for CH_4 dynamics and found that detailed process-based models were not well constrained owing to the complexity of the model. Susiluto et al. (2018) calibrated a detailed model using nine years of EC-based CH_4 flux data in a northern fen. Their results suggested that CH_4 production was the most important factor responsible for the interannual variations in CH_4 emissions, whereas plant-mediated transport was the most important CH_4 transport pathway. Data-model fusion approaches to study CH_4 emissions have been applied only for a limited number of individual sites; thus, their applicability should be evaluated across wide arrays of wetland sites and biomes.

Recently, Ueyama et al. (2022) developed a process-based model (i.e., inferring Processes for Ecosystem-Atmosphere CH_4 Exchange – iPEACE) for partitioning CH_4 emissions using a data-model fusion approach for a cool temperate bog in Japan. Their approach constrained the model using CH_4 emissions and associated biophysical variables from the EC tower with the goal to determine a parameter set for reproducing daily CH_4 emissions under various environmental conditions. These conditions included growing and dormant seasons, wet and dry conditions, high and low LAI, and various ranges of gross primary production (GPP), soil temperature, and PA. The model reasonably identified processes that were qualitatively consistent with previous field experiments to shed light on processes in the bog. Findings include: 1) ebullition and plant-mediated transport as the important CH_4 transport pathways, 2) high contributions of the deep organic layer (i.e., <30 cm) to total CH_4 emissions due to very low CH_4 concentrations in the surface organic layer (Tokida et al., 2007a), and 3) gaseous-bubble accumulation in deep organic layer (Tokida et al., 2005, 2007a, b). A chamber-based study further suggested that contributions of bubble transport to total CH_4 emissions ranged from 67-95% during the snow-free season in the bog (Tokida et al., 2005, 2007a, b), which was close to the iPEACE model estimates (64%).

Here, we modified iPEACE to simulate CH_4 fluxes and infer processes related to CH_4 emissions (i.e., production, oxidation, and transport pathways) from 25 wetlands across mid- to

high-latitudes included in the FLUXNET-CH_4 database. Applying the data-model fusion method (Ueyama et al., 2022) across these wetland sites spanning temperate, boreal, and Arctic regions, our objectives were to: 1) evaluate the model's suitability for simulating CH_4 emissions across wetland types, 2) quantify inter-site variations in estimated processes related to CH_4 emissions, 3) evaluate the sensitivities of CH_4 emissions to GPP, soil temperature, and WTD, and 4) examine inter-site variations in parameters for improved predictions of wetland CH_4 emissions.

2. Materials and methods

2.1 Dataset and model inputs

We used daily EC CH_4 flux data archived in the FLUXNET-CH_4 database (Delwiche et al., 2021). We selected all mid- to high-latitude freshwater wetland sites from the database (Table 2) that contained all relevant forcing variables (i.e., soil and air temperature, WTD, PA, and GPP). The selected 25 sites represent wetland types of bog (ombrotrophic), fen (minerotrophic), marsh, wet tundra, and rice paddy in temperate, boreal, and Arctic regions. The mean annual air temperature ranged from -5 ^{o}C to 17 ^{o}C across the sites, and minimum WTD ranged from -0.62 m to 0.68 m.

We used daily gap-filled CH_4 fluxes and the ancillary biophysical variables at the tower sites. The daily mean values of the gap-filled half-hourly variables were provided in the FLUXNET-CH_4 database (Delwiche et al., 2021). We used two types of daily CH_4 fluxes (i.e., FCH4_F and FCH4_F_ANN_median) in the database. FCH4_F was gap-filled using a multidimensional scaling (MDS) approach in REddyProc (Delwiche et al., 2021), but still contained periods of time with long data gaps (<2 months). FCH4_F_ANN_median was gap-filled based on an artificial neural network method, which fills all data gaps (Knox et al., 2019). As input drivers from the FLUXNET-CH_4 database, daytime-based GPP (GPP_DT) in the database (Lasslop et al., 2010), air temperature (TA_F), barometric pressure (PA_F), soil temperature (TS), and WTD (WTD_F) were used. The gaps in the meteorology (i.e., TA_F, and PA_F) were filled using the ERA-Interim reanalysis data (Vuichard and Papale, 2015), whereas those of WTD and soil temperatures were filled using the MDS method. We used soil temperature at two depths for representing the surface and deep layers in the model. For sites affected by permafrost (RU-Ch2, US-Ics, and US-Uaf), we assumed that the deepest soil temperature measurement was representative of the bottom of the active layer. Data for RU-Ch2, US-Ics, US-Bzf, and US-Bzb sites did not include WTD data in the FLUXNET-CH_4 database, but WTD data were directly provided from principal investigators.

Since WTD for RU-Ch2 was based on discrete manual measurements, we linearly interpolated the data to the daily timescale.

We prepared daily LAI as a model input based on satellite-based LAI smoothed using GPP. First, the four-day LAI data (MCD15A3H; collection 6) was downloaded from MODIS land products subsets. The spatial resolution of the product is 500 m. We used a single grid cell of data centered on the site location. The LAI data were first set to zero for the snow periods, and were then smoothed using a Savitzky-Golay filter (Chen et al., 2004). The snow conditions were determined based on the MODIS reflectance products (MCD43A4; collection 6) from the MODIS land products subsets. Because smoothed LAI often failed to explain seasonal peaks when peak LAI was missing, daily LAI was then modeled using the smoothed LAI and daily GPP normalized with a maximum GPP (*nGPP*). LAI at day (*i*) was modeled with a non-centered moving mean of the normalized GPP multiplying a scale factor.

$$LAI_i = L_s \sum_{j=i-D}^{i} nGPP_j / (D+1) \quad (1)$$

Two empirical parameters of the scale factor for explaining maximum LAI (L_s) and moving window for explaining a lag between GPP and LAI (D) were the parameters determined based on a differential evolution method. Since there was no clear relationship between LAI and GPP for NZ-Kop, LAI for NZ-Kop was estimated simply based on 10-day moving mean of the satellite-based LAI. The smoothed LAI well mimicked the satellite-derived LAI, where mean and standard deviation of root mean square error (RMSE) and correlation coefficient (R) were 0.46 ± 0.24 and 0.84 ± 0.11, respectively, across the sites.

2.2 The iPEACE model

Partitioning CH_4 emissions from the EC measurements was conducted by optimization of a process-based model with the data. We used the iPEACE model (Ueyama et al., 2022), which was originally proposed to infer CH_4 dynamics at a temperate bog in Japan, but has been generalized for the current analysis (Fig. 1).

The iPEACE model consists of two soil layers, a surface layer susceptible to oxic conditions and a deep layer prone to anoxic conditions, and considers CH_4 production and oxidation in each layer, as well as three transport pathways: plant-mediated transport, ebullition, and diffusion. The

modeled mechanisms are similar to those used in current process-based models (Ralvonen et al., 2017; Walter and Heimann, 2000; Wania et al., 2010; Riley et al., 2011). The simple formulation of iPEACE allows to effectively fit the model to data at reduced computational costs. The model is driven with GPP for substrate availability, LAI for transport potential through plant stems, soil temperature in the two layers for driving kinetics, oxygen (O_2) concentration for redox potential, WTD for diffusivity and hydrostatic pressure that drives ebullition, and PA for ebullitive transport. The O_2 concentration was not included in the FLUXNET-CH_4 database, and thus was determined from WTD. When the water table position is above or below a soil layer, the layer is assumed to be anoxic or fully oxic, respectively. When WTD is within a soil layer, O_2 concentration in that layer is linearly related to that fraction of the layer that is inundated between fully oxic to anoxic conditions.

To explore the underlying processes, the model contains 10 parameters and two initial values of the CH_4 pools in each soil layer (mol-CH_4 m^{-3}), which are calibrated with data (Table 3). For adapting the model to the current analysis, the thickness of the surface layer and root fraction (described below) in the surface layer are calibrated for each site, whereas the previous study (Ueyama et al., 2022) used a fixed value.

Thickness of the surface layer (z_{surf}; m) is the parameter constrained by the data. Thickness of the deep layer is calculated as the difference between total soil thickness (1 m, except for permafrost sites) and the thickness of the surface layer. For sites affected by permafrost, total soil thickness is defined as the active layer depth (0.5 m for RU-Ch2, 1.0 m for US-ICs, and 0.6 m for US-Uaf). Seasonal changes in soil thickness associated with soil thaw are not considered in the model for simplicity. Surface root fraction (fs_{root}) is the parameter explaining how roots are concentrated in the surface layer relative to the total roots. The model assumes that root density is higher in the surface layer than the deep layer.

Methane production is assumed to depend on substrate availability from GPP, kinetics as determined by soil temperature, and anaerobic status as determined by O_2 concentration. The fraction of GPP to CH_4 substrate ($p_{production}$; mmol-CH_4 g^{-1} C) and temperature sensitivity (Q_{10}) are both empirical parameters. Modeled CH_4 production increases with soil temperature and substrate availability but decreases with increased O_2 concentration. The $p_{production}$ parameter is the aggregated parameter for explaining the fraction of root exudates from GPP and the efficiency from exudates to CH_4 production and relates to the base production rate in a Q_{10} equation (Chen,

2021). The model does not explicitly consider anaerobic peat decomposition; thus, CH_4 production by decomposition are implicitly incorporated through a decrease in the CH_4 pools. Partitioning of CH_4 substrate in each soil layer is assumed to be a function of the root distribution between the surface and deep soil layers. CH_4 oxidation is calculated with a Michaelis-Menten equation (Wania et al, 2010) with CH_4 concentration and O_2 concentration, where the maximum CH_4 oxidation rate ($p_{oxidation}$; mol-CH_4 m^{-3} s^{-1}) is a calibrated parameter.

Plant-mediated transport is calculated by the concentration gradient between a soil layer and the atmosphere, root fraction in each layer, and LAI. The transfer efficiency under a given concentration gradient (p_{plant}; 10^{-3} d^{-1}) is a calibrated parameter. The model does not consider CH_4 transport by dead plants, which are not accounted for by LAI, with the assumption that collapsed aerenchymatous tissue in senesced leaves has low transport capacity (Korrensalo et al., 2022).

Ebullitive transport is calculated based on a concentration threshold scheme (Peltola et al., 2018), which has two empirical parameters: nondimensional conductivity for bubble transport ($p_{ebullition}$) and a parameter for explaining episodic CH_4 bubble transport driven by barometric pressure changes ($p_{pressure}$; hPa^{-1}). Since the model assumes that CH_4 is not immediately emitted as ebullition but accumulated as bubbles, $p_{ebullition}$ represents the transport efficiency of bubbles. The $p_{pressure}$ parameter empirically explains the sensitivity to decreasing barometric pressure, i.e., the relative increase in ebullition per 1 hPa decrease in mean PA. In the model, the ebullition flux from each layer is assumed to be directly transported to the atmosphere, when WTD is within the top 10 cm of the soil based on a field study (Stanley et al., 2019). When WTD is deeper than 10 cm, CH_4 transport through ebullition is added to the surface layer CH_4 pool, which is a modification from the original model of Ueyama et al. (2022).

Diffusive flux is calculated using Fick's first law. The diffusion coefficients for gas and water are calculated based on Riley et al. (2011), and then their calibrated correction factors ($p_{diffusion\text{-}gas}$ and $p_{diffusion\text{-}water}$) are multiplied to the respective diffusion coefficients.

2.3 Model applications

The model parameters, initial conditions, and model error (σ) were determined from the observed data by the Bayesian method as follows:

$$F_{OBS} \sim Normal(F_{MODEL}, \sigma^2) \quad (2)$$

where the function *Normal* represents the normal distribution, F_{OBS} is the observed CH_4 emission, and F_{MODEL} is the modeled CH_4 emission. The *a priori* distribution of σ was assumed to be a log normal distribution with mean of log(0.5) mg CH_4 m^{-2} d^{-1} and standard deviation of 0.1 mg CH_4 m^{-2} d^{-1}, where the hierarchical structure was used to reduce computational costs. Equation 2 assumes that variance for the model-observation mismatch was temporally uniform without incorporating temporal correlation in the observed data.

The *a priori* distributions of the parameters were generally assumed to be uniform (Table 3). The range of uniform distributions were determined by adding plus/minus to the values determined by the differential evolution method for each site (Table S1). The pre-constraint of *a priori* distribution effectively reduces computational costs without decreasing model performance and improves model convergence, based on a preliminary analysis. For constraining the behavior that root density must be higher in the surface layer than the deep layer in the Bayesian optimization, the thickness of the surface layer and root distribution were determined without results from the mathematical optimization. For the parameter optimization, we did not assume the hierarchy in the statistical model.

The posterior distributions of the parameters were estimated using a Markov Chain Monte Carlo (MCMC) method with the No-U-Turn Sampler (NUTS). NUTS is an extension of Hamiltonian Monte Carlo and provides very effective samples without requiring user intervention or costly tuning runs (Hoffman and Gelman, 2014). The efficiency of NUTS was more than 1,000 times that of Metropolis or Gibbs sampling. Posterior distributions of the parameters were estimated using four chains with 1,000 samples after warm-up based on 1,000 sampling. Bayesian inference was performed using the PyStan library (version 2.19.1.1). Owing to a complex and multimodal parameter space, consistent solutions from each chain were not obtained or some chains were not converged for some sites. In this case, we used results from chains that estimated the lowest model errors. The conservative treatment was required because bad chains seem to converge to local minima rather than to mathematically meaningful multimodal distributions and the problem was not fixed using different *a priori*, different initial values or further sampling. The trace plots and probability density functions for all parameters in all sites are shown in Fig. S1, which shows that at least two chains were well converged. Convergence of MCMC was evaluated by the Gelman–Rubin method with the potential scale reduction factor (PSRF), which showed that

all parameters for all sites were well converged (PSRF < 1.05) except slightly high PSRF for two parameters for US-Uaf (PSRF < 1.12; Table S3). Computational costs of the Bayesian inference ranged from 0.35 hours to 2.5 days per site with an average of 6.16 hours (Table S4).

Model parameters were estimated using daily CH_4 fluxes and the ancillary biophysical variables. Specifically, we used daily gap-filled CH_4 flux (FCH4_F), which contained only long data gaps (>2 months), and did not assume embedded functional relationships. In addition, we used FCH4_F_ANN_median when uncertainties in the neural network (FCH4_uncertainty) were less than absolute of FCH4_F_ANN_median. The use of gap-filled fluxes with low uncertainties could prevent propagating uncertainties associated with long-term gap-filling data into the parameter estimation. We also evaluated how the gap-filled data influenced modeled processes, where we eliminated data records where daily CH_4 emission contained more than 80% gaps in half-hourly data, in constraining the model. Apart from this issue, some high-latitude and rice paddy sites provided only growing-season fluxes, which hampered constraining the model for cold non-growing and fallow seasons, respectively. We also found that flux data for the first few days of a model run were important for constraining the initial CH_4 pools (i.e., initial conditions). Without the data, initial conditions were not well converged, and estimated dormant season emissions were unrealistic. Consequently, when FCH4_F was missing, we used the gap-filled CH_4 flux (FCH4_F_ANN_median) during the first six days of a model run and for the winter period (air temperature < -10 ^{o}C). The benefits of selectively using gap-filled data could outweigh the propagation of gap-filled errors, where unrealistic CH_4 emissions were not estimated.

The model constraints for each site were evaluated by RMSE normalized by mean, R, and normalized standard deviation (SD) in daily CH_4 flux. For further interpreting and analyzing modeled results, we eliminated unconstrained site-data where normalized RMSE was >0.9, R was <0.6, normalized SD was <0.7, or normalized SD was >1.3.

The sensitivities to the forcing variables were performed using the models successfully constrained for each site. First, we applied perturbations to the inputs of: 1) 1 ^{o}C increase to the observed soil temperatures, 2) 10% increase in GPP and LAI, 3) 10 cm increase in WTD, and 4) 10 cm decrease in WTD with all other inputs held at measured conditions. Next, we examined the changes in modeled CH_4 emissions with unperturbed input (control experiment). We conducted the sensitivity analysis for sites spanning at least three years of data because the uncertainties are high in models constrained by short-term data (Ueyama et al., 2022).

To understand the variabilities in the estimated parameters across the sites, we applied principal component analysis (PCA) toward seven parameters: $p_{production}$, $Q_{10production}$, $p_{oxidation}$, $p_{ebullition}$, p_{plant}, $p_{diffusion\text{-}water}$, and $p_{pressure}$. The parameter for gas diffusion ($p_{diffusion\text{-}gas}$) was not included in the PCA because $p_{diffusion\text{-}gas}$ did not show a bell-shaped density curve at approximately half of the sites (Fig. S1). The parameters were first standardized with mean and SD and then compressed into two principal components (PC) using the scikit-learn library in python. We chose two principal components because they explained more than 70% of the variance in the parameters across the sites.

3. Results

3.1. Model performance

Across the 25 sites, 19 sites had reliable performance that satisfied the criterion for normalized RMSE, R, and normalized SD (section 2.3). According to the Taylor diagram (Fig. 2), model-data agreement was the best ($R > 0.9$) for RU-Ch2, FI-Lom, SE-Deg, FI-Sii, and CA-SCB. Among the accepted 19 sites, the median of normalized RMSE, R, and normalized SD were 0.59, 0.82, and 0.87, respectively. Except for the five sites with good model fit noted above, the model underestimated the SD of CH_4 flux, where the mean and SD of the normalized SD was 0.84 ± 0.13 across all sites. For the six sites excluded from subsequent analyses due to low performance (US-Sne, DE-Hte, DE-Zrk, DE-Sfn, US-Bzf, and US-Wpt), the mean seasonality was inconsistent between observations and models (Fig. 3), despite a moderate R and normalized RMSE. The low performance may represent a lack of important processes in the model and insufficient data to constrain the model. For example, US-Sne is a newly restored wetland and has a heterogeneous surface of open water and emergent vegetation, which make it difficult to constrain the processes based only on measured CH_4 fluxes for three years. Overall, there was no significant difference in the model performance in terms of wetland type and the number of years used for calibration.

In general, there were no obvious differences in modeled results with the optimized data containing fully gap-filled data or data when excluding days with >80% gaps. However, five sites (US-Sne, DE-Hte, DE-Zrk, FR-LGt, and NZ-Kop) did not meet the standard for a well constrained model with the non-gap-filled data (Fig. S2). The median of normalized RMSE, R, and normalized SD were 0.57, 0.83, and 0.90, respectively, in the model with the data not containing fully gap-filled data. The estimated CH_4 transport, production, and oxidation were also consistent among the

two models constrained with two data criteria, except for sites having low record numbers (e.g., RU-Ch2 and JP-Mse) (Fig. S3). Other results, including inter-site differences in CH_4 emission processes and sensitivity to biophysical drivers, were generally consistent among the two models constrained with two data criteria.

3.2. Estimated transport processes

Based on model results, plant-mediated transport and ebullition were more important pathways for CH_4 emissions than diffusive transport across sites (Fig. 3, 4; Table 2). In most cases, plant-mediated transport tended to be the major pathway for fen sites (72% ± 10%, n = 8; mean ± SD) and bog sites (55% ± 16%, n = 8; mean ± SD) (Fig. 4). Ebullition accounted for 27% ± 10% of the total emission for the fen sites and 26% ± 10% for the bog sites. In contrast, ebullition was estimated to be the major pathway at the two tundra sites (64% ± 4%) owing to shallow WTD (Fig. 4). Because the modeled plant-mediated transport increased with LAI, relative contribution of ebullition and/or diffusion was found high during periods of low LAI. When LAI was ≥20% of the annual peak, plant-mediated transport was the major pathway (70% ± 14%), except for three sites (RU-Ch2, US-Bzb, and KR-Crk) during the growing season (Fig. 3; Table 2). Diffusion was a minor pathway at most sites, but tended to be high in two marsh sites (US-Myb and US-Tw1) and a bog site (SE-Sto). For the three sites, the model predicted an anoxic surface layer, negligible oxidation, and high CH_4 concentrations in the surface layer at high WTD sites, allowing for surface diffusion. Since US-Myb was a restored wetland, the contribution of diffusion was approximately half of the CH_4 emissions in open water conditions (2010-2011) and then decreased to 31% ± 6% with the expansion of emergent vegetation from 2012 to 2018.

Based on cross-correlation analysis, CH_4 emissions lagged CH_4 production by 1-32 days (Fig. 5). There was more than a 30-day lag between CH_4 production and CH_4 emissions at US-Uaf. Lags tended to be, on average, longer in bogs (13 ± 10 days; n = 7; mean ± SD) than in fens (3 ± 2 days; n = 5), rice paddies (11 ± 3 days; n = 2), or tundra (6 ± 3 days; n = 2). Even in a long-lagged site (> 30 days for US-Uaf), the correlation between CH_4 production and CH_4 emission was good ($R > 0.70$), indicating that CH_4 production controlled temporal variations in CH_4 emission.

Inter-site variations in CH_4 production explained inter-site variations in CH_4 emissions ($R^2 = 0.72$; $p = 0.01$), except for sites where the ratio of oxidation to production was high (Fig. 6a). For sites with high oxidative fraction to production, CH_4 emissions were relatively low considering

their production (Fig. 6a). These sites with high oxidation generally exhibited low minimum WTD (Fig. 6b). CH_4 production and emission were positively correlated with soil temperature and GPP across the sites having low oxidation (Fig. 6c-f). This result is unexpected because the model was constrained in each site using temporal variations in the variables, as there was no assumption about inter-site variations in constraining the model. Based on the variable importance analysis using random forest regression, soil temperature and GPP almost equally explained the inter-site variations in CH_4 production. In contrast to production and oxidation, inter-site variations in three transport pathways did not correlate with CH_4 emissions.

3.3. Estimated parameters

Most parameters in our model were well converged (Table S3), but $p_{diffusion\text{-}gas}$ did not show a bell-shaped density curve with a single peak at 8 of the 19 sites (Fig. S1). Substrates for CH_4 production per GPP ($p_{production}$) were converged on the lower end of *a priori* range (median = 1.1 mmol m^{-2} gC^{-1} m^2) over the 19 sites. The median and SD of Q_{10} of CH_4 production was 3.7 ± 1.9, where there was a weak negative correlation between $p_{production}$ and Q_{10} across the sites (R^2 = 0.31; p = 0.01). The maximum oxidation parameter was estimated to be in the middle of the prescribed upper and lower range at most sites. Estimated $p_{ebullition}$ and p_{plant} were not correlated with contributions from ebullition and plant-mediated transport to CH_4 emission, respectively. Ebullition from 9 sites had a marginal sensitivity to pressure decline (< 2% hPa^{-1}), where there was no correlation between $p_{pressure}$ and contributions of ebullition to the total emission across the sites. There was no significant difference ($p < 0.05$) in all parameters aggregated by aerenchymatous and moss vegetation.

Based on the PCA analysis, 77% of the variance in the parameters among the sites was compressed with two PCs (Fig. 7). The first PC represented a tradeoff of two parameters for CH_4 production between high $p_{production}$ and low Q_{10} and *vice versa*, representing 61% of the parameter distribution across the sites. The second PC explained 16% of the distribution and represented a tradeoff between CH_4 production and transport through plants and gas diffusion. There were weak clusters for bog sites with relatively high Q_{10}, tundra sites with low transport parameters, and rice paddies with high transport parameters. No clusters were apparent for fen and marsh sites.

The thickness of the surface layer, z_{surf}, was the conceptual depth separating surface oxic and deeper anoxic layers, and thus negatively correlated to WTD for sites where minimum WTD was

below -0.1 m (z_{surf} = -1.2 * WTD - 0.05 m; R^2 = 0.48; p=0.03; n = 10). The regression analysis showed that z_{surf} was close to minimum WTD. In contrast, there was no significant trend in the surface layer thickness for sites with high mean annual WTD (> -0.1 m). For sites with high WTD (i.e., always above the ground surface), the thickness of the soil layers did not control the degree of redox conditions for the two layers because the surface layer was always anaerobic.

3.4. Sensitivity to biophysical variables

Based on the sensitivity analysis, CH_4 emissions increased by 9.6% or 3.5 gCH_4 m^{-2} yr^{-1} (median relative increase), with 10% increase in GPP across the sites, with the increases higher in the sites with high annual soil temperatures (Fig. 8a). The sensitivity analysis was performed on sites that had at least three years of data (14 sites) among the 19 sites. The sensitivities aggregated for high or low WTD sites (sites having mean water table position above or below the ground surface) indicated that the relative increases in CH_4 emissions did not differ significantly between the two WTD classes (p = 0.35 in Welch's t test; inset in Fig. 8a).

The 1 ^oC increases in soil temperatures increased CH_4 emissions by 6.6% or 2.5 gCH_4 m^{-2} yr^{-1} (median relative increase) (Fig. 8b). The increases were similar in magnitude to those from the 10% increase in GPP. Compared with the sensitivity to GPP, the increased magnitudes appeared to not be clearly related to the mean annual soil temperatures and WTD, likely because temperature sensitivity (Q_{10}) for CH_4 production differed by site. The increases in CH_4 emissions also did not differ significantly between the two WTD classes (p = 0.80; inset in Fig. 8b).

The increase in CH_4 emissions with 1 ^oC increases were lower than those estimated based on an empirical Q_{10} relationship between daily mean soil temperature and CH_4 emissions (Fig. 9). Eight of the 14 sites were estimated to have higher CH_4 emission sensitivity using the empirical Q_{10} model than iPEACE. Across all 14 sites, the relative increases in CH_4 emissions tended to be higher in the empirical Q_{10} model (12%) than the iPEACE model (8%) across the sites (p = 0.12) (US-Uaf was not included in relative changes in emission owing to the small magnitude in emission).

Decreased CH_4 emissions associated with a 10 cm decrease in WTD were greater than increased CH_4 emissions with a 10 cm increase in WTD (Fig. 8c, d). A decrease in WTD decreased CH_4 emissions at most sites and *vice versa*, where the median changes by the decrease and increase in WTD were -31% and +6.5%, respectively. A site with a WTD permanently well above the

ground surface (US-Myb) did not exhibit significant responses to changing WTD, as WTD always remained above the surface. The relative changes in CH_4 emissions did not differ significantly between sites with low and high WTD with 10 cm increases in WTD (inset in Fig. 8c; $p = 0.34$) and 10 cm decrease in WTD (inset in Fig. 8d; $p = 0.15$).

There were two mechanisms for reduced CH_4 emissions by decreased WTD. The first mechanism is associated with changes in the frequency with which the surface layer becomes oxic conditions. In this mechanism, CH_4 production from the surface layer decreases when the WTD decreases with the perturbed input mostly fluctuating within the surface layer throughout the year. The second mechanism is related to the long-lasting change in redox conditions in the deep layer. We argue that reduced anaerobic conditions in the deep layer, which was rarely affected by oxic conditions with the unperturbed WTD, but was affected by the perturbed decrease in WTD. Owing to the loss of anaerobic conditions, CH_4 in the deep layer was consumed through oxidation; thus, the effects were relatively long-lasting until CH_4 concentrations built-up again. The median decrease in CH_4 production was -6.9 $gCH_4\ m^{-2}\ yr^{-1}$, and median increase in CH_4 oxidation was 12.9 $gCH_4\ m^{-2}\ yr^{-1}$, indicating that the second mechanism was the major process responsible for the reduction in CH_4 emissions. As an exceptional response examined at NZ-Kop, the decreased WTD could change sustained anoxic conditions to oxic conditions in the deep layer, resulting in decreased CH_4 production, reduced CH_4 pool, and finally decreased oxidation.

4. Discussion

The estimated processes for CH_4 emissions provide meaningful insights for interpreting observed data and estimating sensitivities to the forcing variables. The current analysis aims to shed light on the relative importance of processes involved in CH_4 production, transport, and oxidation across 25 freshwater wetland sites in temperate, boreal, and Arctic regions. The observed data included in the FLUXNET-CH_4 database were used to constrain a process-based model which has a similar structure used in previous modeling studies (Walter and Heimann, 2000; Wania et al., 2010; Riley et al., 2011). Flux partitioning is typically applied to net CO_2 fluxes for estimating GPP and ecosystem respiration (Reichstein et al., 2005), and has successfully provided deeper insights on their biotic and abiotic controls (Jung et al., 2017; Mahecha et al., 2010). Compared to the partitioning of CO_2 fluxes, more complex models are required to explain wetland CH_4 emissions and partition net CH_4 flux observations (Wania et al., 2010; Riley et al., 2011; Grant et al., 2019;

Chen 2021). Partitioned CH_4 fluxes can be useful for evaluating inter-site differences in fluxes (Figs. 3, 4), time lags between surface emissions and production (Fig. 5), different responses of CH_4 processes (e.g., production, oxidation, and transport) to biophysical variables (Figs. 6 and 8), and model parameterizations (Fig. 7). Key processes and parameters estimated in this study need to be better constrained with further long-term observations and different data streams.

4.1. Inter-site variations in estimated processes

The inter-site variations in CH_4 emissions were found to be primarily associated with those in CH_4 production rather than those in oxidation and transport (Fig. 6), especially for sites with high WTD and low CH_4 oxidation. These results could explain the correlation of annual CH_4 emissions with mean annual air or soil temperature across global wetlands in the FLUXNET-CH_4 database (Knox et al., 2019; Delwiche et al., 2021), where temperature was found to be an important driver of methanogenesis substrates (Chang et al. 2021) and CH_4 production (Yvon-Durocher et al., 2014). In contrast, oxidation increased with decreasing WTD (Fig. 6b), resulting in oxidation as the second most important process for explaining inter-site variations in CH_4 emissions. These results are also consistent with global syntheses, which showed that a positive correlation between CH_4 emissions and WTD was only detected in sites with relatively low WTD (i.e., mean annual WTD was below the soil surface) (Knox et al., 2019, 2021).

Transport processes were estimated to regulate the time-lag between CH_4 production and emissions (Fig. 5), albeit we found no significant effect on total CH_4 emissions because annual emissions were mainly controlled by CH_4 production (Fig. 6). The lag between production and emission occurred due to the time required to increase the CH_4 concentrations to drive CH_4 transport. The lag of CH_4 emissions to soil temperature or GPP was reported in studies using FLUXNET-CH_4 (Chang et al., 2019; Delwiche et al., 2021; Knox et al., 2021; Yuan et al., 2022). For example, Knox et al. (2021) estimated that on average CH_4 emissions lagged soil temperature and GPP by 5.4 days and 20.7 days, respectively, across wetlands globally. The lag between CH_4 emission and production (Fig. 5) nonetheless partly explained the lag between emission and biophysical variables, as time is required for building up sufficient CH_4 concentrations driving CH_4 emissions.

4.2. Sensitivities of CH_4 emissions to biophysical drivers

572 The estimated sensitivity of CH_4 emissions to GPP (Fig. 8a, b) indicates the importance of
573 substrate availability. A strong relationship between net ecosystem production and CH_4 emissions
574 was previously reported across wetlands extending from subarctic peatlands to subtropical marshes
575 associated with substrate availability (Whiting and Chanton, 1993). The estimated sensitivity
576 occurred because CH_4 production in iPEACE was driven by GPP and soil temperature, reflecting
577 the concept that increased GPP will increase substrate availability and thereby CH_4 emissions. The
578 strong relationship with GPP (Fig. 8a) was unexpected, however, because the sensitivity to GPP
579 ($p_{production}$) was calibrated in each site and thus was expected to show high variability among the
580 sites. It is worth noting that the estimated sensitivity to GPP might be caused by model assumptions.
581 The model assumed that substrates for CH_4 were only provided by GPP, but old peat previously
582 fixed is also known to be a substrate for CH_4 production (Chasar et al., 2000). Substrates from
583 recent primary production and peat organic carbon should be incorporated into future modeling
584 with iPEACE.

585 Based on our sensitivity analyses, CH_4 emissions were sensitive to a decrease in WTD for most
586 sites (Fig. 8). The most important mechanism associated with decreased WTD was increased
587 oxidation at the deep layer. Because the buildup of the CH_4 pool after loss of anaerobic conditions
588 is time consuming, the effects can be long-lasting. This result is consistent with previous studies.
589 Brown et al. (2014) indicated that a long recovery time was required for CH_4 emissions after re-
590 wetting following a drop in WTD at a site where the mean WTD was below the surface. They
591 proposed a reason for the long recovery time as breaking the critical zone for CH_4 emissions by
592 low WTD conditions. Simultaneously, when increased WTD resulted in aerobic layers switching
593 to anaerobic conditions, CH_4 emissions increased, but the response was smaller than those to a
594 decreasing WTD. This difference occurs because increased WTD increased the frequency of
595 anoxic conditions at the surface layer, but the surface layer was still susceptible to oxic conditions
596 even with perturbation increase in WTD, resulting in limited increases in CH_4 concentration. When
597 deep soil remained anaerobic owing to shallow WTD, increases in soil temperature and GPP were
598 equally important drivers of CH_4 emissions through kinetics and substrate availability, respectively
599 (Fig. 8).
600
601 *4.3. Comparison of estimated processes to observations from previous studies*
602 Estimated transport flux was compared to EC measurements at various sites (Table 1). The high

603 ebullition (50% of total emissions) was measured with chamber measurements at JP-Bby (Tokida
604 et al., 2007a, b), which was consistent with the current study. Windham-Myers et al. (2018)
605 measured ebullition with a static chamber during five days in summer at US-Tw1, and ebullition
606 contributions to the total emission (10-30%) were comparable to those by the current study (26%).
607 In contrast, plant-mediated transport estimated with chambers for FI-Sii (31%) and FI-Si2 (21%)
608 was smaller than our model estimates (91% for FI-Sii and 67% for FI-Si2). However, Susiluoto et
609 al. (2018) reported contributions similar to the current study based on process-based models also
610 constrained using EC data (75-95%) for FI-Sii. Kwon et al., (2017) measured lower contributions
611 of plant-mediated transport (25%) and ebullition (2%) in RU-Ch2 than the model estimates.
612 McNicol et al. (2017) measured ebullition by bubble traps (< 1.3%) and diffusion by dissolved
613 CH_4 (< 4.1%) from open water bodies within the flux footprint US-Myb, values which are smaller
614 than the current estimates (18% and 24%, respectively). One reason for the inconsistency might
615 be the spatial heterogeneity at US-Myb. Their study did not consider areas of emergent vegetation
616 where contributions by ebullition can be higher (Villa et al., 2021). Hwang et al. (2020) estimated
617 smaller ebullition (10-17%) than the current study (61%) based on the wavelet analysis of EC data
618 at KR-Crk. For KR-Crk data in the FLUXNET-CH_4 database, WTD under drainage was provided
619 as 0 cm; thus, the model predicted more saturated conditions at the surface than the actual
620 conditions, resulting in higher contributions by ebullition.

621 Based on the site-scale validation, iPEACE estimates were consistent with production,
622 ebullition, or diffusive flux observations at two sites, but inconsistent with observations from four
623 sites. A comprehensive validation of estimated transport fluxes is challenging at the site scale
624 owing to limited sites with both EC data and process studies available at the same location (Table
625 1). Furthermore, no study has in-situ measured the three transport fluxes simultaneously, resulting
626 in uncertainties in how transport fluxes by process studies are consistent with CH_4 emissions
627 measured with EC towers. Plant-mediated transport could be the priority for in-situ measured
628 transport fluxes to validate CH_4 emissions, since it was estimated to be a major pathway in most
629 sites (Table 2) and in other modeling studies (Table 1). Differences in spatial representativeness
630 between EC towers and process studies could also contribute to inconsistencies.

631 Our estimated wetland CH_4 emissions were within the range of those measured or predicted
632 with process-based models regardless of difficulties in direct comparisons at the site scale.
633 Although the contributions of each transport flux were highly variable among previous studies

(Table 1), plant-mediated transport and ebullition tended to be major transport pathways, consistent with our current estimates (Fig. 4). Previous models also estimated plant-mediated transport as the major pathway (Table 1), although the VISIT model predicted ebullition as the major pathway for Arctic wetlands (Ito, 2019). In contrast, iPEACE tended to estimate higher contributions from ebullition and lower contributions from diffusion. This difference could be caused by the assumption that ebullition occurs when WTD is greater than 10 cm below the ground (Stanley et al., 2019). The contribution of plant-mediated transport was similar to previous modeling studies because of similar model structure, but tended to be higher than measurements (Table 1). Rhizospheric oxidation (Bansal et al., 2020; Korrensalo et al., 2022) is a potential reason for low CH_4 emissions through vegetation, which was not considered in the current version of iPEACE.

4.4. Toward refined parameterizations

Based on the PCA (Fig. 7), modeling wetland CH_4 emissions could be improved with refined parameterization and representation of CH_4 production, plant-mediated transport, and diffusion through water. The importance of parameterizations for production and plant-mediated transport was also estimated in a study constraining a global CH_4 model with observed CH_4 emissions at 16 wetland sites (Müller et al., 2015). The high explanatory power in the first PC by the production parameters suggests that CH_4 production was important for inter-site variations in CH_4 emissions. Considering the structure of iPEACE, sites with high $p_{production}$ could be more limited by substrate availability, whereas sites with high Q_{10} could be more limited by kinetics. The second PC explained CH_4 emissions that are limited by production and/or transport. A similar trade-off between parameters of production and plant-mediated transport was also inferred in an optimized process-based model (Salmon et al., 2022). These results suggest that a model for explaining variabilities in parameters of production and plant-mediated transport across wetlands is needed for refined simulations rather than determining one set of parameters.

4.5. Next steps in modeling wetland CH_4 emissions

The estimated processes were the most likely processes for explaining observed CH_4 emissions under the model structure of iPEACE (section 2.2), suggesting that careful interpretation is required. iPEACE considers important processes to explain CH_4 emissions that have been

incorporated in some previous modeling studies (Walter and Heimann, 2000; Wania et al., 2010; Riley et al., 2011). However, definitions and formulations of CH_4-related processes are often different among models (Melton et al., 2013). For instance, iPEACE does not include processes included in more mechanistic models (e.g., Salmon et al., 2022; Susiluto et a., 2018). We need to better define processes in the model and to validate modeled processes, where the model-data fusion could be useful to bridge model and observation.

To improve our understanding of CH_4 emissions from wetlands, future improvements are possible with increased availability of EC data, additional observations, and by incorporating more processes into the model. First, in-situ observations of transport fluxes and production parameters with incubations would be useful to constrain the model because Bayesian optimization can effectively incorporate the additional constraints from observations. Second, more long-term data are required for better constraining the model. The period of the current study ranged from one to nine years with a median of four years. Ueyama et al. (2022) indicated that long-term data (e.g., >3 years) effectively constrained the partitioned fluxes. Furthermore, we did not focus on tree-dominated wetlands (e.g., swamps) owing to the importance of unaccounted processes, such as CH_4 transport to the atmosphere by tree stems (Pangala et al., 2012), or from O_2 transport to the rhizosphere via aerial roots (Purvaja et al., 2004). In this study, we predicted O_2 concentration in the soil based on WTD, but the relationship between O_2 concentrations and WTD is complex (Ueyama et al., 2020). Thus, measurements of WTD and O_2 concentrations are strongly recommended for evaluating CH_4 emissions in wetlands. The current model considers a 1 m thick soil, but anaerobic peat deeper than 1 m could play a role in CH_4 emissions (Tokida et al., 2007a, b; Peltola et al., 2018). Since flux tower measurements did not continuously monitor the O_2 and CH_4 concentrations in the deep peat, constraining processes at the deep peat were difficult in this study. Finally, refined modeling wetland CH_4 emission will be possible by evaluating how partitioned emissions are consistent across different models constrained with the same data.

The Bayesian inference in this study might be improved after considering the outlined limitations. We did not obtain reliable results for 6 of 23 sites. The inability could be caused by lack of important processes, but might be resolved with improved mathematical techniques. The error distribution was assumed with Gaussian distribution, which lacked the ability to fit long-tail, such as data containing outliers. Use of other error distributions might improve posterior inference (Hamura et al., 2022). For 12 sites, at least one chain was not well converged (Fig. S1), possibly

due to a problem of slow convergence associated with complex multimodal parameter distributions. Introducing Extended Ensemble Monte Carlo (Iba, 2001), such as the replica exchange method, could improve convergence. The techniques for complex parameter distributions could improve the parameter optimization, where some parameters in the current study hit the range of prior distributions (Fig. S1) possibly owing to the equifinality problem (Schulz et al., 2001).

Acknowledgements

We acknowledge support from the John Wesley Powell Center for Analysis and Synthesis of the U.S. Geological Survey (USGS)("Wetland FLUXNET Synthesis for Methane" working group, https://www.usgs.gov/centers/john-wesley-powell-center-for-analysis-and-synthesis/science/wetland-fluxnet-synthesis) and the USGS Ecosystem Mission Area, Land Change Science programs. We thank Dr. Eric J Ward for providing useful comments on the manuscript. ESE was supported by the grants from the Arctic Observatory Program of the National Science Foundation (grant numbers 1936752, 1503912, 1107892) and by the US Geological Survey, Research Work Order 224 to the University of Alaska Fairbanks, the Bonanza Creek Long-Term Ecological Research Program funded by the National Science Foundation (NSF DEB-1026415, DEB-1636476) and the NSF Long-Term Research in Environmental Biology Program (NSF LTREB 2011276). MU was supported by the Arctic Challenge for Sustainability II (ArCS II; JPMXD1420318865) and JSPS KAKENHI (20K21849). IM was supported by ICOS-Finland, Academy of Finland project N-PERM and Horizon Europe project GreenFeedBack. MK was supported by the Rural Development Administration (PJ014892022022). TS was supported by the Helmholtz Association of German Research Centres (VH-NG-821). DE-Zrk is a Terrestrial Environmental Observatories Network (TERENO) site. SD was supported by the U.S. Geological Survey, Ecosystems Mission Area, Land Change Science Program. SG was supported by the SNO Tourbières, CNRS-INSU. OS was supported by the Canada Research Chairs, Canada Foundation for Innovation Leaders Opportunity Fund, and Natural Sciences and Engineering Research Council Discovery Grant Programs. WJR and KYC were supported by the Reducing Uncertainties in Biogeochemical Interactions through Synthesis and Computation (RUBISCO) Scientific Focus Area, Office of Biological and Environmental Research of the U.S. Department of Energy Office of Science. YR was supported by the Ministry of Environment of Korea (2022003640002). Lawrence Berkeley National Laboratory (LBNL) is managed by the University

of California for the U.S. Department of Energy under contract DE-AC02-05CH11231, California Department of Water Resources, CA Fish and Wildlife, and US DOE Ameriflux. Any use of trade, firm, or product names is for descriptive purposes only and does not imply endorsement by the U.S. Government.

Data availability statement

The data that support the findings of this study are available in the FLUXNET-CH_4 Community Product, available at https://fluxnet.org/data/fluxnet-ch4-community-product/. DOIs for individual site data are provided in Table 2. The iPEACE source code is available upon request to the authors.

References

Baldocchi, D. (2014). Measuring fluxes of trace gases and energy between ecosystems and the atmosphere – the state and future of the eddy covariance method. Global Change Biology, 20, 3600-3609.

Bansal, S., Johnson, O. F., Meier, J., & Zhu, X. (2020). Vegetation affects timing and location of wetland methane emissions. Journal of Geophysical Research: Biogeosciences, 125, e2020JG005777.

Bohn T. J., Melton, J. R., Ito, A., Kleinen, T., Spahni, R., Stocker, B. D., Zhang, B., Zhu, X., Schroeder, R., Glagolev, M. V., Maksyutov, S., Brovkin, V., Chen, G., Denisov, S. N., Eliseev, A. V., Gallego-Sala, A., McDonald, K. C., Rawlins, M. A., Riley, W. J., … Kaplan, J. O. (2015). WETCHIMP-WSL: intercomparison of wetland methane emissions models over West Siberia. Biogeosciences, 12, 3321-3349.

Bridgham, S. D., Cadillo-Quiroz, H., Keller, J. K., & Zhuang, Q. (2013). Methane emissions from wetlands: biogeochemical, microbial, and modeling perspectives from local to global scales. Global Change Biology, 19, 1325-1346.

Brown, M. G., Humphreys, E. R., Moore, T. R., Roulet, N. T., & Lafleur, P. M. (2014). Evidence for a nonmonotonic relationship between ecosystem-scale peatland methane emissions and water table depth. Journal of Geophysical Research Biogeosciences, 119, 826-835.

Butterbach-Bahl, K., Papen, H., & Rennenberg, H. (1997). Impact of gas transport through rice cultivars on methane emission from rice paddy fields. Plant, Cell and Environment, 20, 1175-1183.

Campbell, D., & Goodrich, J. (2020). FLUXNET-CH_4 NZ-Kop Kopuatai. New Zealand. https://doi.org/10.18140/FLX/1669652

Castro-Morales, K., Kleinen, T., Kaiser, S., Zaehle, S., Kittler, F., Kwon, M. J., Beer, C., & Göckede, M. (2018). Year-round simulated methane emissions from a permafrost ecosystem in Northeast Siberia,

759 Biogeosciences, 15, 2691-2722.
760 Chang, K.-Y., Riley, W., Knox, S., Jackson, R., McNicol, G., Poulter, B., Aurela, M., Baldocchi, D., Bansal,
761 S., Bohrer, G., Campbell, D., Cescatti, A., Chu, H., Delwiche, K., Desai, A., Euskirchen, E., Friborg,
762 T., Gockede, M., Helbig, M., … Zona, D. (2021). Substantial hysteresis in emergent temperature
763 sensitivity of global wetland CH_4 emissions. Nature Communications, 12, 2266.
764 Chang, K.-Y., Riley, Crill, P. M., Grant, R. E., & Saleska, S. R. (2020). Hysteretic temperature sensitivity
765 of wetland CH_4 fluxes explained by substrate availability and microbial activity. Biogeosciences, 17,
766 5849-5860.
767 Chasar, L. S., Chanton, J. P., Glaser, P. H., Siegel, D. I., & Rivers, J. S. (2000). Radiocarbon and stable
768 carbon isotopic evidence for transport and transformation of dissolved organic carbon, dissolved
769 inorganic carbon, and CH_4 in a northern Minnesota peatland. Global Biogeochemical Cycles, 14, 1095-
770 1108.
771 Chen, J. (2021). *Biophysical Models and Applications in Ecosystem Analysis*. Michigan State University
772 Press.
773 Chen, J., & Chu, H. (2020). FLUXNET-CH_4 US-WPT Winous Point North Marsh. United States.
774 https://doi.org/10.18140/FLX/1669702
775 Chen, J., Jönsson, P., Tamura, M., Gu, Z., Matsushita, B., & Eklundh, L. (2004). A simple method for
776 reconstructing a high-quality NDVI time-series data set based on the Savitzky–Golay filter. Remote
777 Sensing of Environment, 91, 332-344.
778 Chu, H., Chen, J., Gottgens, J. F., Ouyang, Z., John, R., Czajkowski, K., & Becker, R. (2014). Net
779 ecosystem methane and carbon dioxide exchanges in a Lake Erie coastal marsh and a nearby
780 cropland. *Journal of Geophysical Research: Biogeosciences*, *119*(5), 722-740.
781 Conrad, R. (2009). The global methane cycle: recent advance in understanding the microbial processes
782 involved. Environmental Microbiology Reports, 1, 285-292.
783 Delwiche, K. B., Knox, S. H., Malhotra, A., Fluet-Chouinard, E., McNicol, G., Feron, S., Ouyang, Z.,
784 Papale, D., Trotta, C., Canfora, E., Cheah, Y.-W., Christianson, D., Alberto, M. C. R., Alekseychik, P.,
785 Aurela, M., Baldocchi, D., Bansal, S., Billesbach, D. P., Bohrer, G., … Jackson, R. B. (2021).
786 FLUXNET-CH_4: A global, multi-ecosystem dataset and analysis of methane seasonality from
787 freshwater wetlands. Earth System Science Data, 13, 3607-3689.
788 Desai, A. R. (2020). FLUXNET-CH_4 US-Los Lost Creek. United States.
789 https://doi.org/10.18140/FLX/1669682
790 Dorodnikov, M., Knorr, K.-H., Kuzyakov, Y., & Wilmking, M. (2011). Plant-mediated CH_4 transport and
791 contribution of photosynthates to methanogenesis at a boreal mire: a ^{14}C pulse-labeling study.
792 Biogeosciences, 8, 2365-2375.

Eichelmann, E., Knox, S., Rey-Sanchez, A. C., Valach, A., Sturtevant, C., Szutu, D., Verfaillie, J., & Baldocchi, D. (2020). FLUXNET-CH_4 US-Tw4 twitchell east end wetland. United States. https://doi.org/10.18140/FLX/1669698

Euskirchen, E., Bret-Harte, M., & Edgar, C. (2020). FLUXNET-CH_4 US-ICs Imnavait Creek Watershed Wet Sedge Tundra, United States. https://doi.org/10.18140/FLX/1669678

Euskirchen, E., & Edgar, C. (2020a). FLUXNET-CH_4 US-BZF Bonanza Creek Rich Fen, United States. https://doi.org/10.18140/FLX/1669669

Euskirchen, E., & Edgar, C. (2020b). FLUXNET-CH_4 USBZB Bonanza Creek Thermokarst Bog, United States. https://doi.org/10.18140/FLX/1669668

Glaser, P. H., Morin, C. P., Rosenberry, D. O., Siegel, D. I., Ruud, O., Chasar, L. I., & Reeve, A. S. (2004). Surface deformations as indicators of deep ebullition fluxes in a large northern peatland. Global Biogeochemical Cycles 19, GB1003, doi:10.1029/2003GB002069.

Goeckede, M. (2020). FLUXNET-CH_4 RU-Ch2 Chersky reference, Russian Federation. https://doi.org/10.18140/FLX/1669654

Göckede, M., Kittler, F., & Schaller, C., (2019). Quantifying the impact of emission outbursts and non-stationary flow on eddy covariance CH_4 flux measurements using wavelet techniques. Biogeosciences, 16, 3113-3131.

Gogo, S., Guimbaud, C., Laggoun-Défarge, F., Catoire, V., & Robert, C. (2011). In situ quantification of CH_4 bubbling events from a peat soil using a new infrared laser spectrometer. Journal of Soils Sediments, 11, 545-551.

Grant, R. F., Mekonnen, Z. A., Riley, W. J., Arora, B., & Torn, M. S., (2019). Modeling climate change impacts on an arctic polygonal tundra: 2. changes in CO_2 and CH_4 exchange depend on rates of permafrost thaw as affected by changes in vegetation and drainage. Journal of Geophysical Research: Biogeosciences, 124, 1323-1341.

Hamura, Y., Irie, K., Sugasawa, S., (2022). Log-regularly varying scale mixture of normals for robust regression. Computational Statistics & Data Analysis, 173, 107517.

Hoffman, M. D., & Gelman, A., (2014). The No-U-Turn sampler: adaptively setting path lengths in Hamiltonian Monte Carlo. Journal of Machine Learning Research, 15, 1593-1623.

Hwang, Y., Ryu, Y., Huang, Y., Kim, J., Iwata, H., & Kang, M. (2020). Comprehensive assessments of carbon dynamics in an intermittently-irrigated rice paddy. Agricultural and Forest Meteorology, 285-286, 107933.

Iba, Y., (2001). Extended Ensemble Monte Carlo. International Journal of Modern Physics C, 12, 623-656.

Ito, A. (2019). Methane emission from pan-Arctic natural wetlands estimated using a process-based model, 1901–2016. Polar Science, 21, 26-36.

827 Iwata, H. (2020). FLUXNET-CH_4 JP-Mse Mase rice paddy field. Japan.
828 https://doi.org/10.18140/FLX/1669647
829 Iwata, H., Hirata, R., Takahashi, Y., Miyabara, Y., Itoh, M., & Iizuka, K. (2018). Partitioning eddy-
830 covariance methane fluxes from a shallow lake into diffusive and ebullitive fluxes. Boundary-Layer
831 Meteorology, 169, 416-428.
832 Iwata, H., Ueyama, M., & Harazono, Y. (2020). FLUXNET-CH_4 US-Uaf University of Alaska, Fairbanks.
833 United States. https://doi.org/10.18140/FLX/1669701
834 Jackson, R. B., Saunois, M., Bousquet, P., Canadell, J. G., Poulter, B., Stavert, A. R., Bergamaschi, P.,
835 Niwa, Y., Segers, A., & Tsuruta, A. (2020). Increasing anthropogenic methane emissions arise equally
836 from agricultural and fossil fuel sources. Environmental Research Letters, 15, 071002
837 Jacotot, A., Gogo, S., & Laggoun-Défarge, F. (2020). FLUXNET-CH_4 FR-LGt La Guette, France.
838 https://doi.org/10.18140/FLX/1669641
839 Jung, M., Reichstein, M., Schwalm, C. R., Huntingford, C., Sitch, S., Ahlström, A., Arneth, A., Camps-
840 Valls, G., Ciais, P., Friedlingstein, P., Gans, F., Ichii, K., Jain, A. K., Kato, E., Papale, D., Poulter, B.,
841 Raduly, B., Rödenbeck, C., Tramontana, G., … Zeng, N. (2017). Compensatory water effects link
842 yearly global land CO_2 sink changes to temperature. Nature, 541, 516-520.
843 Kajiura, M., & Tokida, T. (2021). Quantifying bubbling emission (ebullition) of methane from a rice paddy
844 using high-time-resolution concentration data obtained during a closed-chamber measurement. Journal
845 of Agricultural Meteorology, 77, 245-252.
846 Karofeld, E., & Tónisson, H. (2014). Spatio-temporal changes in bog pool bottom topography – temperature
847 effect and its influence on pool development: an example from a raised bog in Estonia. Hydrological
848 Processes 28:958-968.
849 Knox, S. H., Jackson, R. B., Poulter, B., McNicol, G., Fluet-Chouinard, E., Zhang, Z., Hugelius, G.,
850 Bousquet, P., Canadell, J. G., Saunois, M., Papale, D., Chu, H., Keenan, T. F., Baldocchi, D., Torn, M.
851 S., Mammarella, I., Trotta, C., Aurela, M., Bohrer, G., … Zona, D. (2019). FLUXNET-CH_4 synthesis
852 activity: objective, observations, and future directions. Bulletin of the American Meteorological
853 Society, 100, 2607-2632.
854 Knox, S. H., Bansal, S., McNicol, G., Schafer, K., Sturtevant, C., Ueyama, M., Valach, A. C., Baldocchi,
855 D., Delwiche, K., Desai, A. R., Euskirchen, E., Liu, J., Lohila, A., Malhotra, A., Melling, L., Riley, W.,
856 Runkle, B. R. K., Turner, J., Vargas, R., … Jackson, R B. (2021). Identifying dominant environmental
857 predictors of freshwater wetland methane fluxes across diurnal to seasonal time scales. Global Change
858 Biology, 27, 3582-3604.
859 Koebsch, F., & Jurasinski, G. (2020). FLUXNET-CH_4 DE-Hte Huetelmoor. Germany.
860 https://doi.org/10.18140/FLX/1669634

Koebsch, F., Jurasinski, G., Koch, M., Hofmann, J., & Glatzel, S. (2015). Controls for multi-scale temporal variation in ecosystem methane exchange during the growing season of a permanently inundated fen. Agricultural and Forest Meteorology, 204, 94-105.

Korrensalo, A., Mammarella, I., Alekseychik, P., Vesala, T., & Tuittila, E-S. (2022). Plant mediated methane efflux from a boreal peatland complex. Plant Soil, 471, 375-392.

Kutzback, L., Wagner, D., & Pfeiffer, E.-M., (2004). Effect of microrelief and vegetation on methane emission from wet polygonal tundra, Lena Delta, Northern Siberia. Biogeochemistry 69:341-362.

Kwon, M. J., Beulig, F., Ilie, I., Wildner, M., Küsel, K., Merbold, L., Mahecha, M. D., Zimov, N., Zimov, S. A., Heimann, M., Schuur, E. A. G., Kostka, J. E., Kolle, O., Hilke, I., & Göckede, M. (2017). Plants, microorganisms, and soil temperatures contribute to a decrease in methane fluxes on a drained Arctic floodplain, Global Change Biology, 23, 2396-2412.

Lasslop, G., Reichstein, M., Papale, D., Richardson, A. D., Arneth, A., Barr, A., Stoy, P., & Wohlfahrt, G. (2010). Separation of net ecosystem exchange into assimilation and respiration using a light response curve approach: critical issues and global evaluation, Global Change Biology, 16, 187–208.

Lohila, A., Aurela, M., Tuovinen, J.-P., Laurila, T., Hatakka, J., Rainne, J., & Mäkelä, T. (2020). FLUXNET-CH_4 FI-Lom Lompolojankka. Finland. https://doi.org/10.18140/FLX/1669638

Ma, S., Jiang, J., Huang, Y., Shi, Z., Wilson, R. M., Ricciuto, D., Sebestyen, S. D., Hanson, P. J., & Luo, Y. (2017). Data-constrained projections of methane fluxes in a Northern Minnesota peatland in response to elevated CO_2 and warming. Journal of Geophysical Research: Biogeosciences, 122, 2841-2861.

Mahecha, M. D., Reichstein, M., Carvlhais, N., Lasslop, G., Lange, H., Seneviratne, S. I., Vargas, R., Ammann, C., Arain, M. A., Cescatti, A., Janssens, I. A., Migliavacca, M., Montagnani, L., & Richardson, A. D. (2010). Global convergence in the temperature sensitivity of respiration at ecosystem level. Science, 329, 838-840.

Männistö, E., Korrensalo, A., Alekseychik, P., Mammarella, I., Peltola, O., Vesala, T., & Tuittila, E.-S., (2019). Multi-year methane ebullition measurements from water and bare peat surfaces of a patterned boreal bog. Biogeosciences 16:2409-2421.

Matthes, J. H., Sturtevant, C., Oikawa, P., Chamberlain, S. D., Szutu, D., Ortiz, A. A., Verfaillie, J., & Baldocchi, D. (2020). FLUXNET-CH_4 US-Myb Mayberry Wetland. United States. https://doi.org/10.18140/FLX/1669685

McNicol, G., Sturtevant, C. S., Knox, S. H., Dronova, I., Baldocchi, D. D., & Silver, W. L. (2017). Effects of seasonality, transport pathway, and spatial structure on greenhouse gas fluxes in a restored wetland. Global Change Biology 23:2768-2782.

Melton, J. R., Wania, R., Hodson, E. L., Poulter, B., Ringeval, B., Spahni, R., Bohn, T., Avis, C. A.,

Beerling, D. J., Chen, G., Eliseev, A. V., Denisov, S. N., Hopcroft, P. O., Lettenmaier, D. P., Riley, W. J., Singarayer, J. S., Subin, Z. M., Tian, H., Zürcher, S., … Kaplan, J. O. (2013). Present state of global wetland extent and wetland methane modelling: conclusions from a model inter-comparison project (WETCHIMP). Biogeosciences, 10, 753-788.

Moore, T. R., & Roulet, N. T. (1993). Methane flux: water table relations in northern wetlands. Geophysical Research Letter, 20, 587-590.

Morin, T. H. (2018). Advances in the eddy covariance approach to CH_4 monitoring over two and a half decades. Journal of Geophysical Research: Biogeosciences, 124, 453-460.

Morrissey, L. A., & Livingston, G. P. (1992). Methane emissions from Alaska Arctic tundra: An assessment of local spatial variability. Journal of Geophysical Research: Atmospheres 97:16661-16670.

Müller, J., Paudel, R., Shoemaker, C. A., Woodbury, J., Wang, Y., & Mahowald, N. (2015). CH_4 parameters estimation in CLM4.5bgc using surrogate global optimization. Geoscientific Model Development, 8, 3285-3310.

Nilsson, M. B., & Peichl, M. (2020). FLUXNET-CH_4 SE-Deg Degero. Sweden. https://doi.org/10.18140/FLX/1669659

Pangala, S. R., Moore, S., Hornibrook, E. R. C., & Gauci, V. (2013). Trees are major conduits for methane egress from tropical forested wetlands. New Phytolotist, 197, 524-531.

Pastorello, G., Trotta, C., Canfora, E., Chu, H., Christianson, D., Cheah, Y.-W., Poindexter, C., Chen, J., Elbashandy, A., Humphrey, M., Isaac, P., Polidori, D., Reichstein, M., Ribeca, A., van Ingen, C., Vuichard, N., Zhang, L., Amiro, B., Ammann, C., …Law, B. (2020). The FLUXNET2015 dataset and the ONEFlux processing pipeline for eddy covariance data. Scientific Data, 7, 225. https://www.nature.com/articles/s41597-020-0534-3

Peltola, O., Raivonen, M., Li, X., & Vesala, T. (2018). Technical note: comparison of methane ebullition modelling approaches used in terrestrial wetland models. Biogeosciences, 15, 937-951.

Purvaja, R., Ramesh, R., & Frenzel, P. (2004). Plant-mediated methane emission from an Indian mangrove. Global Change Biology, 10, 1825–1834.

Raivonen, M., Smolander, S., Backman, L., Susiluoto, J., Aalto, T., Markkanen, T., Mäkelä, J., Rinne,J., Peltola,O., Aurela, M., Lohila, A., Tomasic, M., Li, X., Larmola, T., Juutinen, S., Tuittila, E-.S., Heimann, M., Sevanto, S., Kleinen, T. Brovkin, V., Vesala, T. (2017). HIMMELI v1.0: HelsinkI Model of MEthane buiLd-up and emIssion for peatlands. Geoscientific Model Development, 10, 4665-4691.

Reichstein, M., Falge, E., Baldocchi, D., Papale, D., Aubinet, M., Berbigier, P., Bernhofer, C., Buchmann, N., Gilmanov, T., Granier, A., Grünwald, T., Havránková, K., Ilvesniemi, H., Janous, D., Knohl, A., Laurila, T., Lohila, A., Loustau, D., Matteucci, G., … Valentini, R. (2005). On the separation of net ecosystem exchange into assimilation and ecosystem respiration: review and improved algorithm.

929 Global Change Biology, 11, 1-16.
930 Richardson, W. P., Reba, M. L., & Runkle, B. R. (2022). Modification of wavelet-based method for
931 detecting ebullitive methane fluxes in eddy-covariance observations: application at two rice fields.
932 Boundary-Layer Meteorology 184:71-111.
933 Riley, W. J., Subin, Z. M., Lawrence, D. M., Swenson, S. C., Torn, M. S., Meng, L., Mahowald, N. M., &
934 Hess, P. (2011). Barriers to predicting change in global terrestrial methane fluxes: analyses using
935 CLM4Me, a methane biogeochemistry model integrated in CESM. Biogeosciences, 8, 1925-1953.
936 Rinne, J., Tuittila, E.-S., Peltola, O., Li, X., Raivonen, M., Alekseychik, P., Haapanala, S., Pihlatie, M.,
937 Aurela, M., Mammarella, I., & Vesala, T. (2018). Temporal variation of ecosystem scale methane
938 emission from a boreal fen in relation to temperature, water table position, and carbon dioxide fluxes.
939 Global Biogeochemical Cycles, 32, 1087-1106.
940 Ryu, Y., Kang, M., & Kim, J. (2020). FLUXNET-CH_4 KR-CRK Cheorwon Rice paddy. Republic of Korea.
941 https://doi.org/10.18140/FLX/1669649
942 Sachs, T., & Wille, C. (2020). FLUXNET-CH_4 DE-Zrk Zarnekow. Germany.
943 https://doi.org/10.18140/FLX/1669636
944 Salmon, E., Jégou, F., Guenet, B., Jourdain, L., Qiu, C., Bastrikov, V., Guimbaud, C., Zhu, D., Ciais, P.,
945 Peylin, P., Gogo, S., Laggoun-Défarge. F., Aurela, M., Bret-Harte, M. S., Chen, J., Chojnicki, B. H.,
946 Chu, H., Edgar, C. W., …Ziemblińska, B. (2022). Assessing methane emissions for northern peatlands
947 in ORCHIDEE-PEAT revision 7020. Geoscientific Model Development, 15, 2813-2838.
948 Santoni, G. W., Lee, B. H., Goodrich, J. P., Vammer, R. K., Crill, P. M., McManus, J. B., Nelson, D. D.,
949 Zahniser, M. S., & Wofsy, S. C. (2012). Mass fluxes and isofluxes of methane (CH_4) at a New
950 Hampshire fen measured by a continuous wave quantum cascade laser spectrometer. Journal of
951 Geophysical Research 117, D10301, doi:10.1029/2011JD016960
952 Saunois, M., Stavert, A. R., Poulter, B., Bousquet, P., Canadell, J. G., Jackson, R. B., Raymond, P. A.,
953 Dlugokencky, E. J., Houweling, S., Patra, P. K., Ciais, P., Arora, V. K., Bastviken, D., Bergamaschi,
954 P., Blake, D. R., Brailsford, G., Bruhwiler, L., Carlson, K. M., Carrol, M., … Zhuang, Q. (2020). The
955 global methane budget 2000–2017. Earth System Science Data, 12(3), 1561–1623.
956 https://doi.org/10.5194/essd-12-1561-2020
957 Schaller, C., Kittler, F., Foken, T., & Göckede, M., (2019). Characterisation of short-term extreme methane
958 fluxes related to non-turbulent mixing above an Arctic permafrost ecosystem. Atmospheric. Chemistry
959 and Physics, 19, 4041-4059.
960 Schmid, H. P., & Klatt, J. (2020). FLUXNET-CH_4 DE-SfN Schechenfilz Nord, Germany.
961 https://doi.org/10.18140/FLX/1669635
962 Schulz, K., Jarvis, A., & Beven, K. (2001). The predictive uncertainty of land surface fluxes in response to

963 increasing ambient carbon dioxide. Journal of Climate, 14, 2551-2562.
964 Shannon, R. D., White, J. R., Lawson, J. E., & Gilmour, B. S., (1996). Methane efflux from emergent
965 vegetation in peatlands. Journal of Ecology 84:239-246.
966 Shortt, R., Hemes, K., Szutu, D., Verfaillie, J., & Baldocchi, D. (2020). FLUXNET-CH_4 US-Sne Sherman
967 Island Restored Wetland, United States. https://doi.org/10.18140/FLX/1669693
968 Sonnentag, O., & Helbig, M. (2020). FLUXNET-CH_4 CA-SCB Scotty Creek bog. Canada.
969 https://doi.org/10.18140/FLX/1669613
970 Stamp, I., Baird, A. J., & Heppell, C. M. (2013). The importance of ebullition as a mechanism of methane
971 (CH_4) loss to the atmosphere in a northern peatland. Geophysical Research Letters 40:2087-2090.
972 Stanley, K. M., Heppell, C. M., Belyea, L. R., Baird, A. J., & Field, R. H. (2019). The importance of CH_4
973 emission in floodplain fens. Journal of Geophysical Research: Biogeosciences, 124, 1750-1763.
974 Sturtevant, C. S., Ruddell, B. L., Knox, S. H., Verfaillie, J., Matthes, J. H., Oikawa, P. Y., & Baldocchi, D.
975 (2016). Identifying scale-emergent, nonlinear, asynchronous processes of wetland methane exchange.
976 Journal of Geophysical Research: Biogeosciences, 121, 188-204.
977 Susiluoto, J., Raivonen, M., Backman, L., Laine, M., Peltola, O., Vesala, T., & Aalto, T. (2018). Calibrating
978 the sqHIMMELI v1.0 wetland methane emission model with hierarchical modeling and adaptive
979 MCMC. Geoscientific Model Development, 11, 1199-1228.
980 Tokida, T., Miyazaki, T., & Mizoguchi, M. (2005). Ebullition of methane from peat with falling
981 atmospheric pressure. Geophysical Research Letters, 32, L13823, doi:10.1029/2005GL022949.
982 Tokida, T., Miyazaki, T., Mizoguchi, M., Nagata, F., Takakai, F., Kagemoto, A., & Hatano, R. (2007a).
983 Falling atmospheric pressure as a trigger for methane ebullition from peatland. Global Biogeochemical
984 Cycles, 23, GB2003. doi:10.1029/2006GB002790.
985 Tokida, T., Mizoguchi, M., Miyazaki, T., Kagemoto, A., Nagata, O., & Hatano, R. (2007b). Episodic
986 release of methane bubbles from peatland during spring thaw. Chemosphere, 70, 165-171.
987 Turetsky, M. R., Kotowska, A., Bubier, J., Dise, N. B., Crill, P., Hornibrook, E. R. C., Minkkinen, K.,
988 Moore, T. R., Myers-Smith, I. H., Nykänen, H., Olefeldt, D., Rinne, J., Saarnio, S., Shurpali, N., Tuittila,
989 E.-S., Waddington, J. M., White, J. R., Wickland, K. P., & Wilmking, M. (2014). A synthesis of
990 methane emissions from 71 northern, temperate, and subtropical wetlands. Global Change Biology, 20,
991 2183-2197.
992 Ueyama, M., Hirano, T., & Kominami, Y. (2020). FLUXNET-CH_4 JP-BBY Bibai bog. Japan.
993 https://doi.org/10.18140/FLX/1669646
994 Ueyama, M., Yazaki, T., Hirano, T., & Endo, R. (2022). Partitioning methane flux by the eddy covariance
995 method in a cool temperate bog based on a Bayesian framework. Agricultural and Forest Meteorology,
996 316, 08852.

997 Ueyama, M., Yazaki, T., Hirano, T., Futakuchi, Y., & Okamura, M. (2020). Environmental controls on
998 methane fluxes in a cool temperate bog. Agricultural and Forest Meteorology, 281, 107852.
999 Valach, A., Szutu, D., Eichelmann, E., Knox, S., Verfaillie, J., & Baldocchi, D. (2020). FLUXNET-CH_4
1000 US-Tw1 twitchell wetland west pond. United States. https://doi.org/10.18140/FLX/1669696
1001 Vesala, T., Tuittila, E.-S., Mammarella, I., & Alekseychik, P. (2020a). FLUXNET-CH_4 FI-Si2 Siikaneva-
1002 2 Bog. Finland. https://doi.org/10.18140/FLX/1669639
1003 Vesala, T., Tuittila, E.-S., Mammarella, I., & Rinne, J. (2020b). FLUXNET-CH_4 FI-Sii Siikaneva. Finland.
1004 https://doi.org/10.18140/FLX/1669640
1005 Villa, J. A., Ju, Y., Stephen, T., Rey-Sanchez, C., Wrighton, K. C., & Bohrer, G. (2020). Plant-mediated
1006 methane transport in emergent and floating-leaved species of a temperate freshwater mineral-soil
1007 wetland. Limnology and Oceanography, 65, 1635-1650. https://doi.org/10.1002/lno.11467
1008 Villa, J. A., Ju, Y., Yazbeck, T., Waldo, S., Wrighton, K. C., & Bohrer, G. (2021). Ebullition dominates
1009 methane fluxes from the water surface across different ecohydrological patches in a temperate
1010 freshwater marsh at the end of the growing season. Science of the Total Environment 767:
1011 Vuichard, N., & Papale, D. (2015). Filling the gaps in meteorological continuous data measured at
1012 FLUXNET sites with ERA-Interim reanalysis. Earth System Science Data, 7, 157-171.
1013 Walter, P. B., & Heimann, M. (2000). A process-based, climate-sensitive model to derive methane
1014 emissions from natural wetlands: application to five wetland sites, sensitivity to model parameters, and
1015 climate. Global Biogeochemical Cycles, 14, 745-765.
1016 Wania, R., Ross, I., & Prentice, I. C. (2010). Implementation and evaluation of a new methane model within
1017 a dynamic global model: LPJ-WHyMe v1.3.1. Geoscientific Model Development, 3, 565-584.
1018 Whiting, G. J., & Chanton, J. P. (1993). Primary production control of methane emission from wetlands.
1019 Nature, 364, 794-795.
1020 Windham-Myers, L., Bergamaschi, B., Anderson, F., Knox, S., Miller, R., & Fujii, R. (2018). Potential for
1021 negative emissions of greenhouse gases (CO_2, CH_4 and N_2O) through coastal peatland re-establishment:
1022 Novel insights from high frequency flux data at meter and kilometer scales. Environmental Research
1023 Letters, 13, 045005.
1024 Yuan, K., Zhu, Q., Li, F., Riley, W. J., Torn, M. S., Chu, H., McNicol, G., Chen, M., Knox, S. H., Delwiche,
1025 K., Wu, H., Baldocchi, D., Ma, H., Desai, A., Chen, J., Sachs, T., Ueyama, M., Sonnentag, O., Helbig,
1026 M., Tuittila, E., Jurasinski, G., Koebsch, F., Campbell, D., Schmid, H. P., Lohila, A., Goeckede, M.,
1027 Nilsson, M. B., Friborg, T., Jansen, J., Zona, D., Euskirchen, E., Krauss, K. W., Bohrer, G., Jin, Z., Liu,
1028 L., Iwata, H., Goodrich, J. P., & Jackson, R. (2022). Causality guided machine learning model on
1029 wetland CH_4 emissions across global wetlands. Agricultural and Forest Meteorology, 324, 109115.
1030 Yvon-Durocher, G., Allen, A. P., Bastviken, D., Conrad, R., Gudasz, C., St-Pierre, A., Thanh-Duc, N., &

1031 del Giorgio, P. A. (2014). Methane fluxes show consistent temperature dependence across microbial to
1032 ecosystem scales. Nature, 507, 488-491.
1033

Figures and table captions

Fig. 1. Schematic representation of the model structure for methane (CH_4) flux. The model consists of two soil layers: a surface layer susceptible to oxic conditions and a deep layer prone to anoxic conditions. Ecosystem-atmosphere CH_4 fluxes are the net result of CH_4 production ($p_{production}$ and Q_{10}), oxidation ($p_{oxidation}$), and transport processes. Transport is the sum of diffusion ($p_{diffusion-gas}$ and $p_{diffusion-water}$), plant-mediated transport (p_{plant}), and ebullition ($p_{ebullition}$ and $p_{pressure}$). Substrate for CH_4 production associated with gross primary productivity (GPP) is divided into surface and deep layers (z_{surf}), considering root distribution (f_{root}). The model is driven by biophysical variables: soil temperature (Ts) in the two soil layers, water table depth (WTD), leaf area index (LAI), GPP, and barometric pressure (PA). Calibrated parameters are shown with parentheses, and dashed lines represent a major flow of causality.

Fig. 2. Taylor diagram of the model performances in daily methane (CH_4) fluxes for each site. The benchmark corresponding to observations is shown as Obs with red dots. RMSE = root mean square error.

Fig. 3. Mean seasonal variations of observed and modeled methane (CH_4) fluxes and the transport components of plant-mediated transport, ebullition, and diffusion. The seasonality is calculated as a mean across years, and then a seven-day moving mean is applied for smoothing. Note differences in y-axis ranges among panels. Frames colored by blue are the sites having acceptable model performance (normalized root mean square error was >0.9, correlation coefficient was <0.6, normalized standard deviation was <0.7, or normalized standard deviation was >1.3), and those colored by brown are the sites having low performance.

Fig. 4. Ternary plot for modeled annual methane (CH_4) transport pathways of plant-mediated transport, ebullition, and diffusion.

Fig. 5. Lag time between modeled methane (CH_4) production and CH_4 flux based on a cross-correlation analysis, plotted against the correlation coefficient between CH_4 fluxes and lagged CH_4 production.

Fig. 6. Relationships between modeled methane (CH_4) production and CH_4 flux (a), between minimum water table position and ratio of oxidation to production (b), between mean annual soil temperature and modeled CH_4 production (c), between gross primary productivity (GPP) and modeled CH_4 production (d), between soil temperature and modeled CH_4 flux (e), and between GPP and CH_4 flux (f). Annual mean or minimum for the study period are shown. Blue lines in (a, c, d, e, f) represent linear regression (all $p < 0.001$) based on sites where modeled oxidation contributed less than 70% of CH_4 production, where shading represents the prediction interval ($p = 0.1$). Dashed line in (a) represents the 1:1 line between production and flux. The high CH_4 production for NZ-Kop (525 mg CH_4 m^{-2} d^{-1}) is too high to fit the range in the figure (a, c, d). Points represent mean values over the observation period, and their colors represent the ratio of CH_4 oxidation to production.

Fig. 7. Biplots showing the first and second components based on the principal components (PC) of the estimated parameters across the sites: methane (CH_4) production per gross primary productivity ($p_{production}$), Q_{10} for CH_4 production, maximum CH_4 oxidation rate ($p_{oxidation}$), nondimensional conductivity for gaseous transfer ($p_{ebullition}$), diffusion coefficient for plant-mediated transport (p_{plant}), diffusion coefficient multiplier for water ($p_{diffusion\text{-}water}$), and sensitivity of ebullition to barometric pressure ($p_{pressure}$).

Fig. 8. Modeled sensitivity of annual mean methane (CH_4) flux to perturbed input of 10% high gross primary productivity (GPP) (a), biased input of 1°C high soil temperatures (Ts) (b), 10 cm high water table position (WTP) (c), and 10 cm low WTP (d). The changes in fluxes were shown on climate space of mean annual soil temperature and mean annual WTP over the observation period for each site. Boxplots represent the relative changes in flux for aggregated sites having annual high and low mean WTP (higher and lower above the ground, respectively), where dots represent outliers. The relative changes by boxplots did not include US-Uaf, because the flux was too low and the ratio was anomalously high due to low denominator. The sensitivity analysis was done for sites having at least three years of data.

Fig. 9. Change in methane (CH_4) flux estimated with a perturbed input of 1°C increase in soil temperatures for the empirical Q_{10} model and iPEACE model. The colors in plots represent the

empirical Q_{10} value between daily CH_4 flux and soil temperature for the surface layer. Boxplots represent the relative changes in flux for aggregated sites having annual high and low mean water table positions (higher and lower above the ground, respectively). The relative changes by boxplots did not include US-Uaf, because the flux was too low and the ratio was anomalously high due to low denominator.

Table 1. Literature survey for partitioned methane (CH_4) emissions from wetlands (i.e., ebullition diffusion, and plant-mediated transport) based on field observations and modeling.

Table 2. Description of study sites, showing wetland type, location, dominant vegetation type (DOM_VEG), mean annual air temperature (TAVE), GPP, annual maximum monthly leaf area index (LAI) (MCD15A3H), mean annual soil temperature (TS), water table depth during the period when soil was thaw (WTD gs), and modeled partitioned methane (CH_4) emissions during the growing season when LAI was higher than 20% of the annual maximum.

Table 3. Ranges of parameters for mathematical optimization and prior distributions for Bayesian optimization for the iPEACE model. The range of uniform distributions were determined by adding plus/minus to the values determined by the differential evolution method for each site (Table S1).

Figure 1

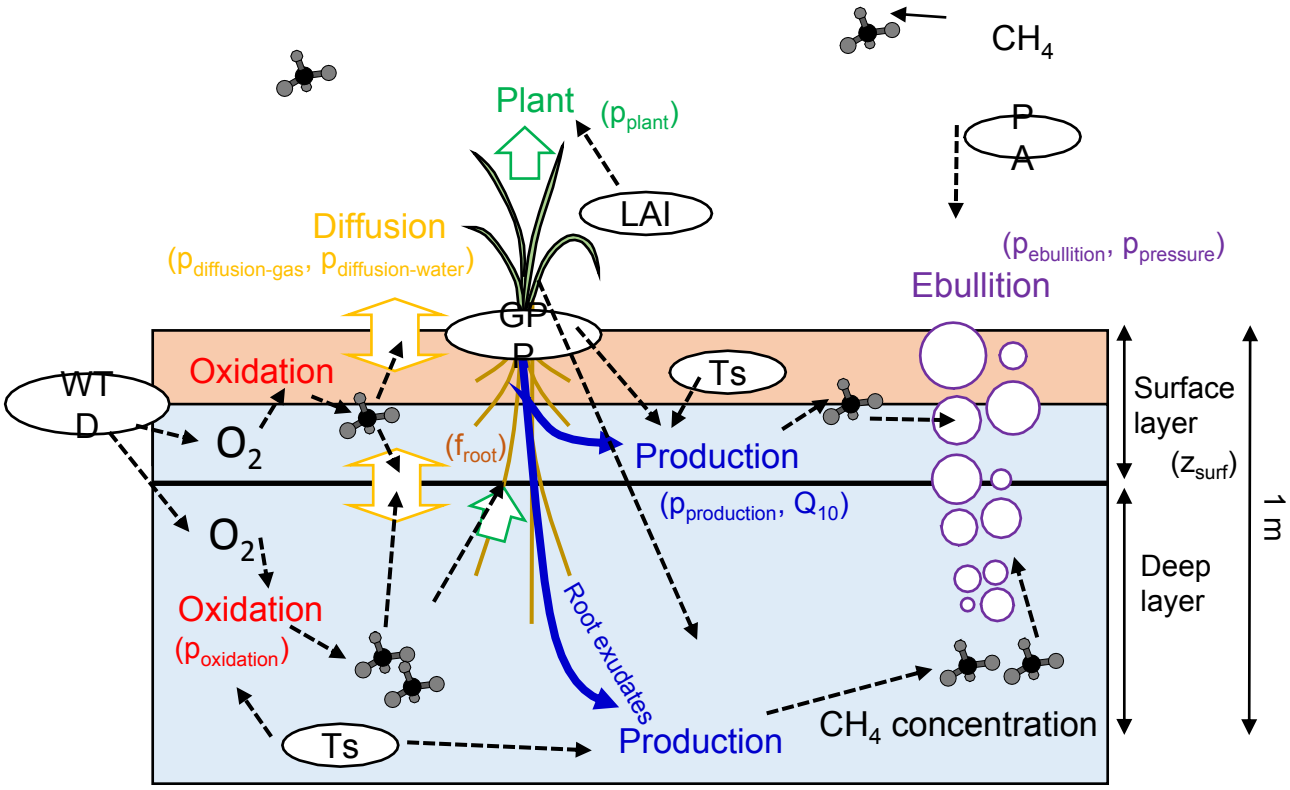

Schematic representation of the model structure for methane (CH_4) flux. The model consists of two soil layers: a surface layer susceptible to oxic conditions and a deep layer prone to anoxic conditions. Ecosystem-atmosphere CH_4 fluxes are the net result of CH_4 production ($p_{production}$ and Q_{10}), oxidation ($p_{oxidation}$), and transport processes. Transport is the sum of diffusion ($p_{diffusion\text{-}gas}$ and $p_{diffusion\text{-}water}$), plant-mediated transport (p_{plant}), and ebullition ($p_{ebullition}$ and $p_{pressure}$). Substrate for CH_4 production associated with gross primary productivity (GPP) is divided into surface and deep layers (z_{surf}), considering root distribution (f_{root}). The model is driven by biophysical variables: soil temperature (Ts) in the two soil layers, water table depth (WTD), leaf area index (LAI), GPP, and barometric pressure (PA). Calibrated parameters are shown with parentheses, and dashed lines represent a major flow of causality.

Figure 2

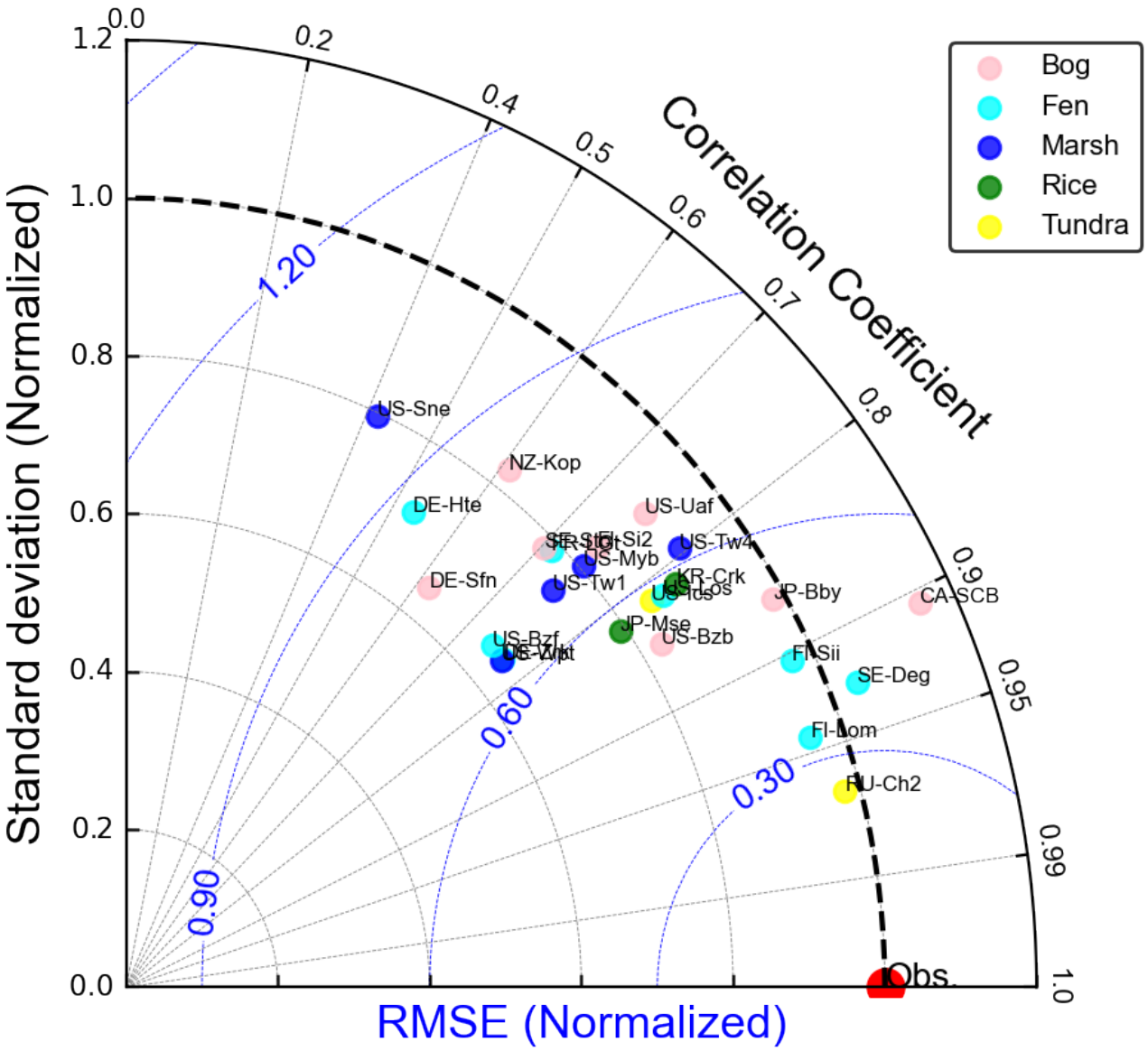

Taylor diagram of the model performances in daily methane (CH_4) fluxes for each site. The benchmark corresponding to observations is shown as Obs with red dots. RMSE = root mean square error.

Figure 3

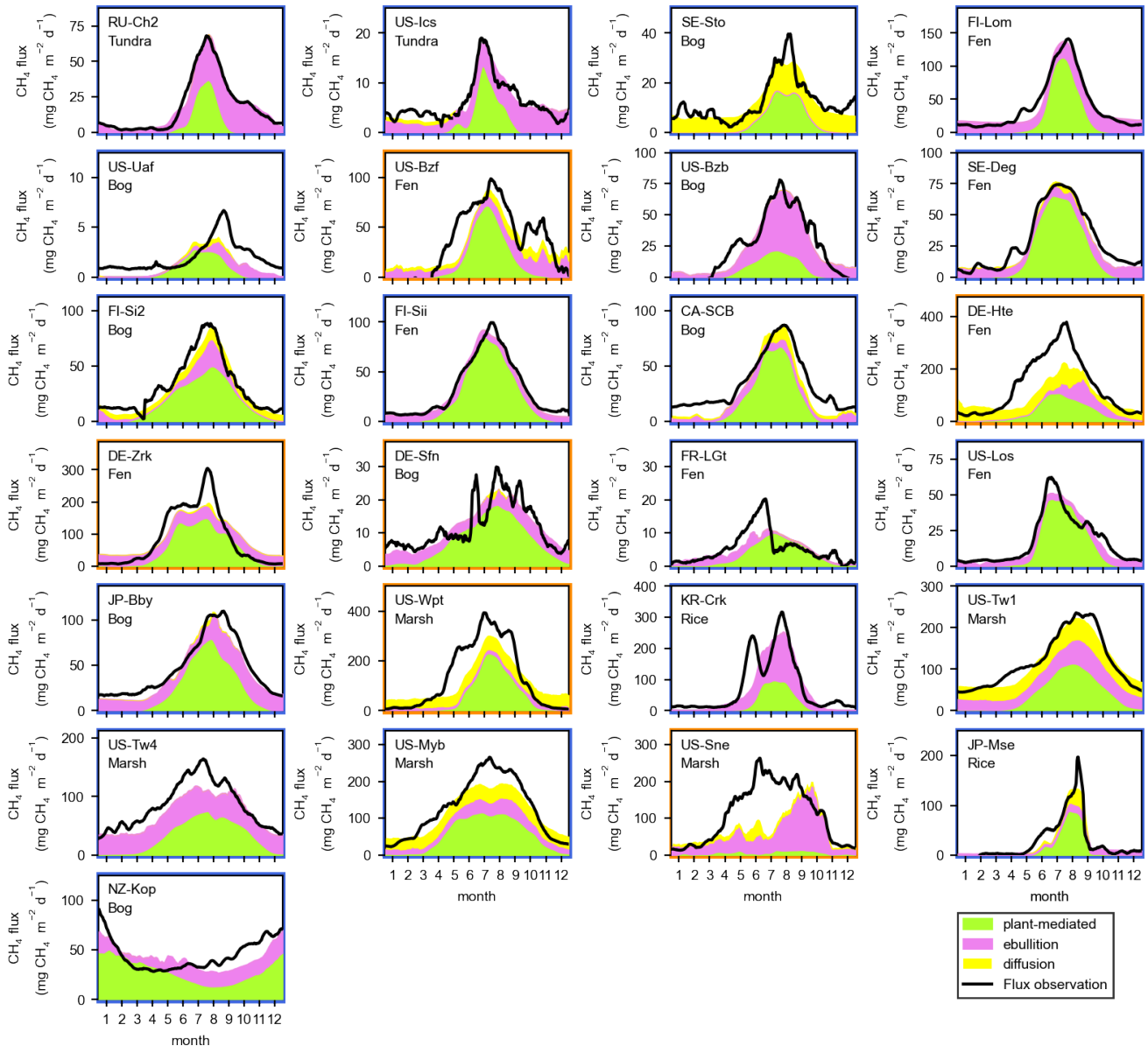

Mean seasonal variations of observed and modeled methane (CH_4) fluxes and the transport components of plant-mediated transport, ebullition, and diffusion. The seasonality is calculated as a mean across years, and then a seven-day moving mean is applied for smoothing. Note differences in y-axis ranges among panels. Frames colored by blue are the sites having acceptable model performance (normalized root mean square error was >0.9, correlation coefficient was <0.6, normalized standard deviation was <0.7, or normalized standard deviation was >1.3), and those colored by brown are the sites having low performance.

Figure 4

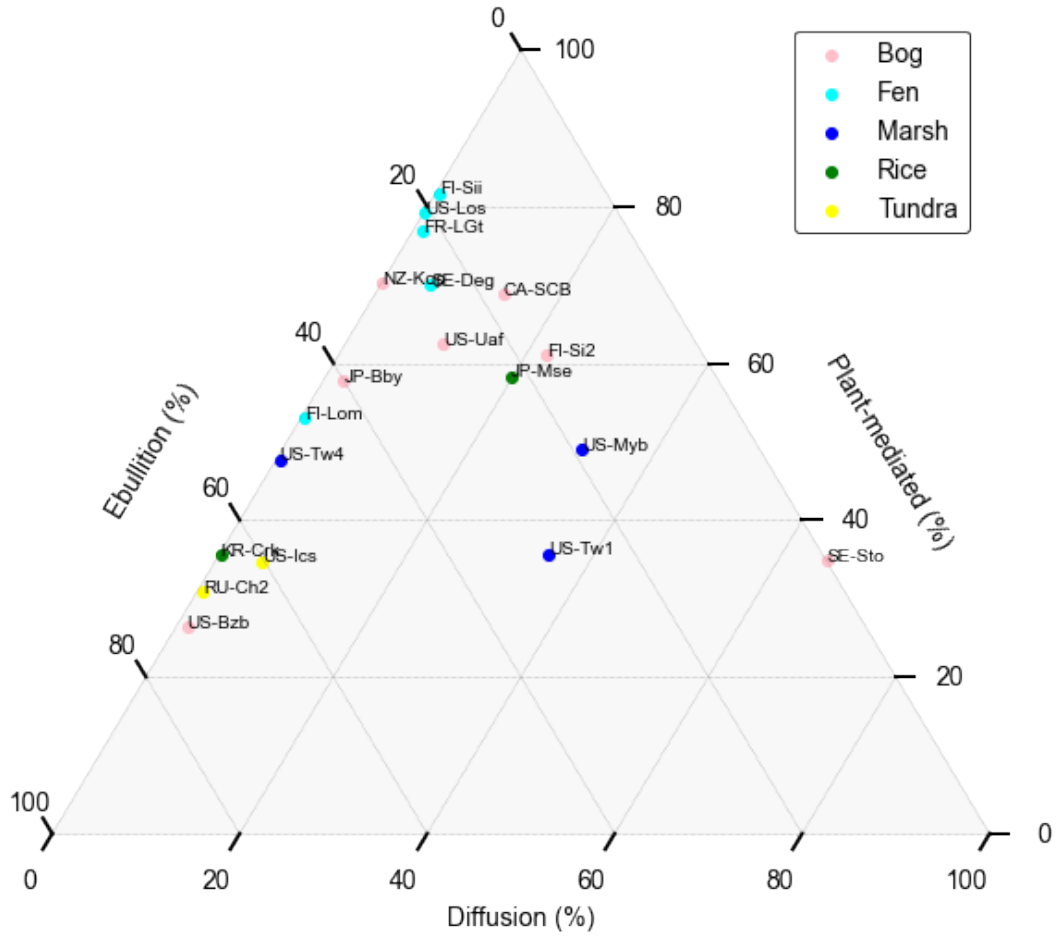

Ternary plot for modeled annual methane (CH_4) transport pathways of plant-mediated transport, ebullition, and diffusion.

Figure 5

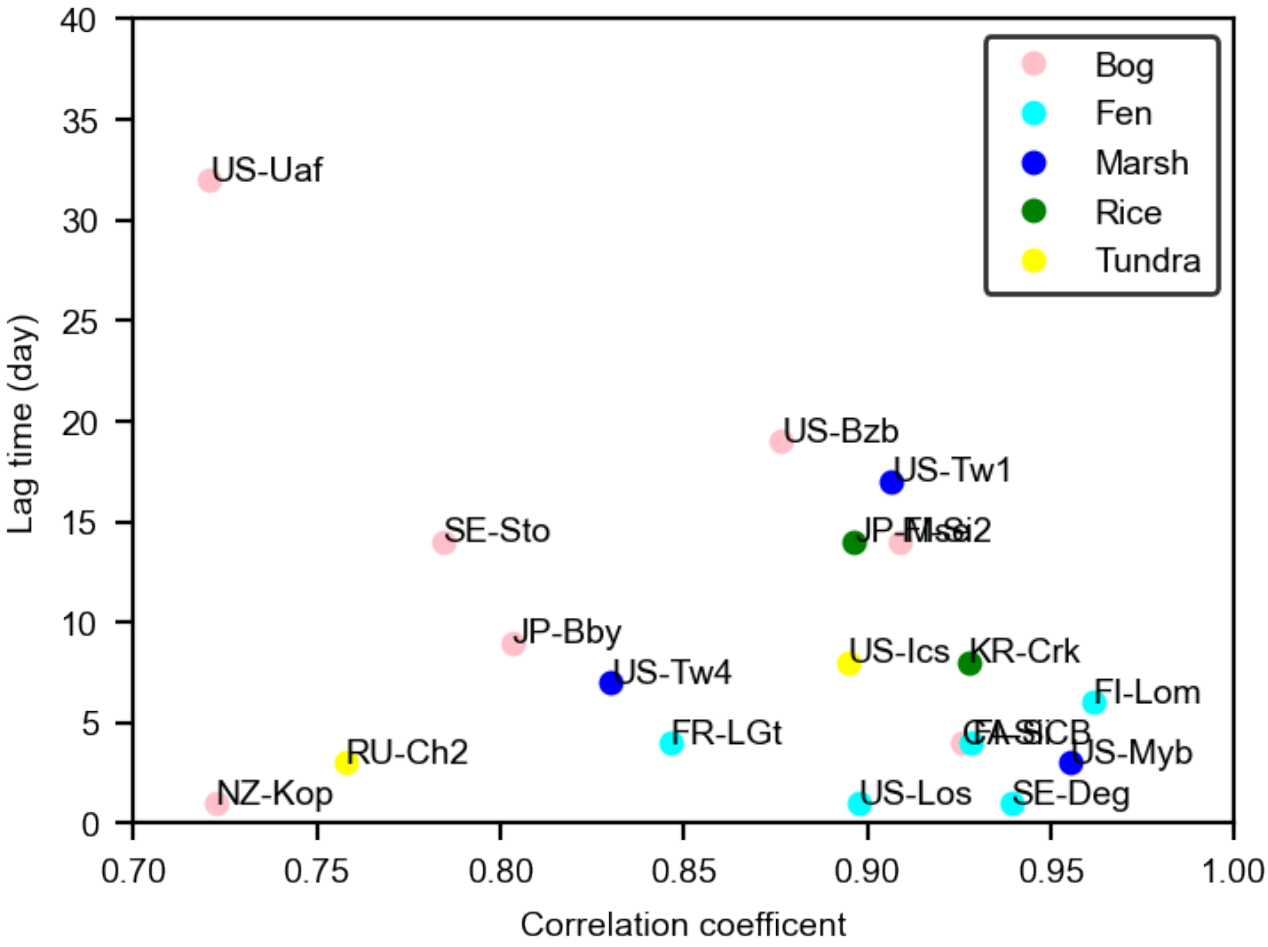

Lag time between modeled methane (CH_4) production and CH_4 flux based on a cross-correlation analysis, plotted against the correlation coefficient between CH_4 fluxes and lagged CH_4 production.

Figure 6

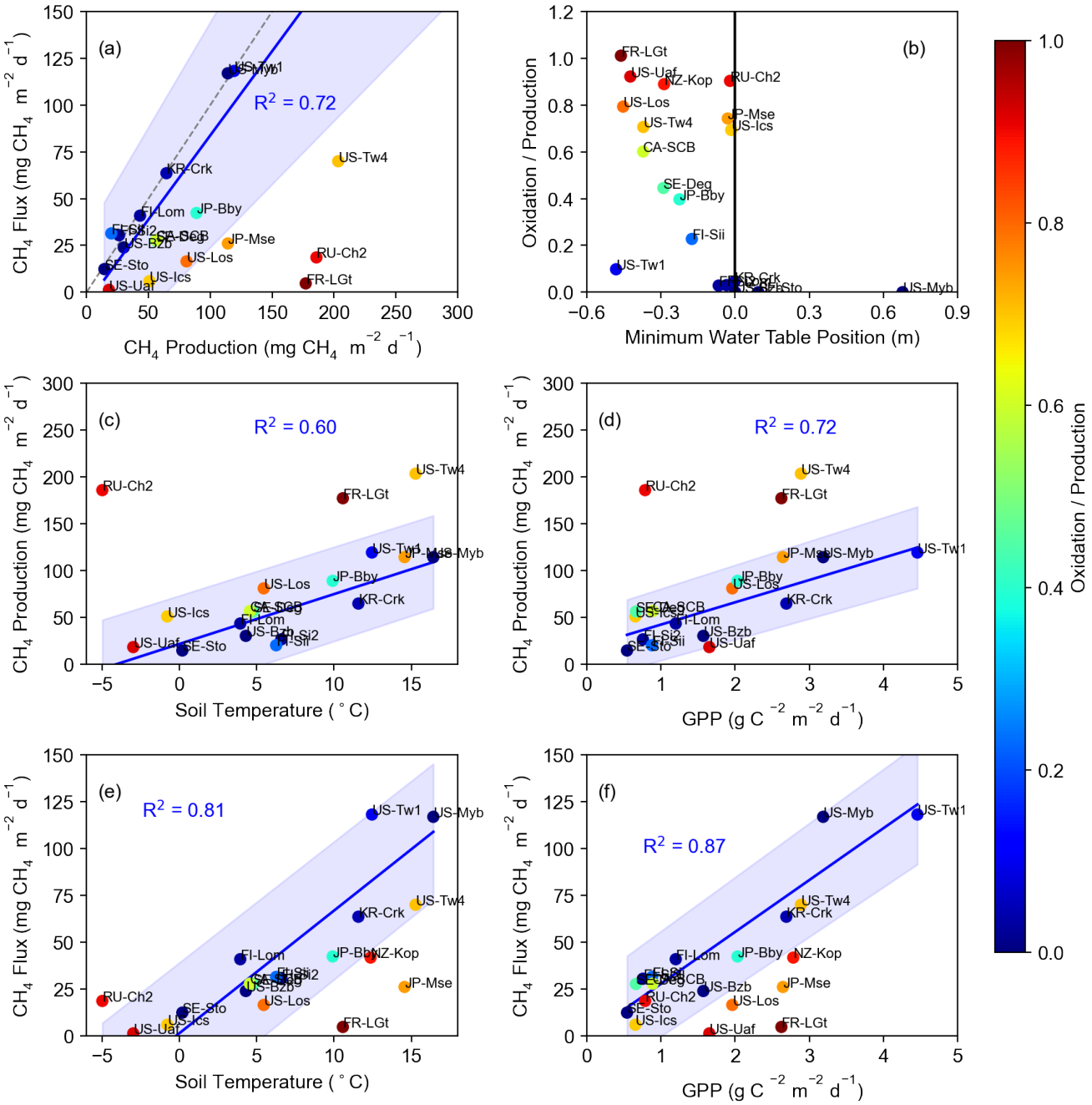

Relationships between modeled methane (CH_4) production and CH_4 flux (a), between minimum water table position and ratio of oxidation to production (b), between mean annual soil temperature and modeled CH_4 production (c), between gross primary productivity (GPP) and modeled CH_4 production (d), between soil temperature and modeled CH_4 flux (e), and between GPP and CH_4 flux (f). Annual mean or minimum for the study period are shown. Blue lines in (a, c, d, e, f) represent linear regression (all $p < 0.001$) based on sites where modeled oxidation contributed less than 70% of CH_4 production, where shading represents the prediction interval ($p = 0.1$). Dashed line in (a) represents the 1:1 line between production and flux. The high CH_4 production for NZ-Kop (525 mg CH_4 m^{-2} d^{-1}) is too high to fit the range in the figure (a, c, d). Points represent mean values over the observation period, and their colors represent the ratio of CH_4 oxidation to production.

Figure 7

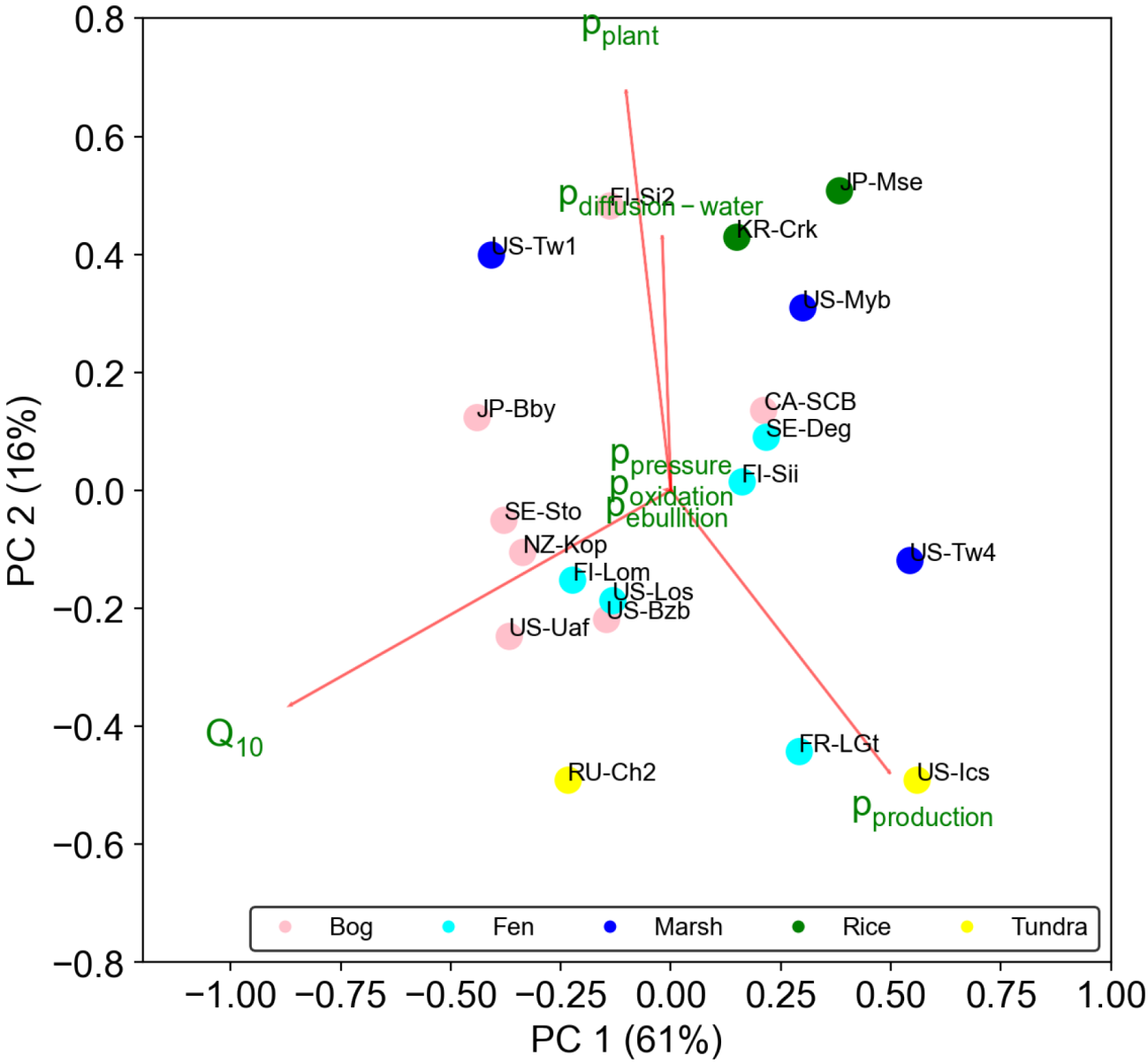

Biplots showing the first and second components based on the principal components (PC) of the estimated parameters across the sites: methane (CH_4) production per gross primary productivity ($p_{production}$), Q_{10} for CH_4 production, maximum CH_4 oxidation rate ($p_{oxidation}$), nondimensional conductivity for gaseous transfer ($p_{ebullition}$), diffusion coefficient for plant-mediated transport (p_{plant}), diffusion coefficient multiplier for water ($p_{diffusion\text{-}water}$), and sensitivity of ebullition to barometric pressure ($p_{pressure}$).

Figure 8

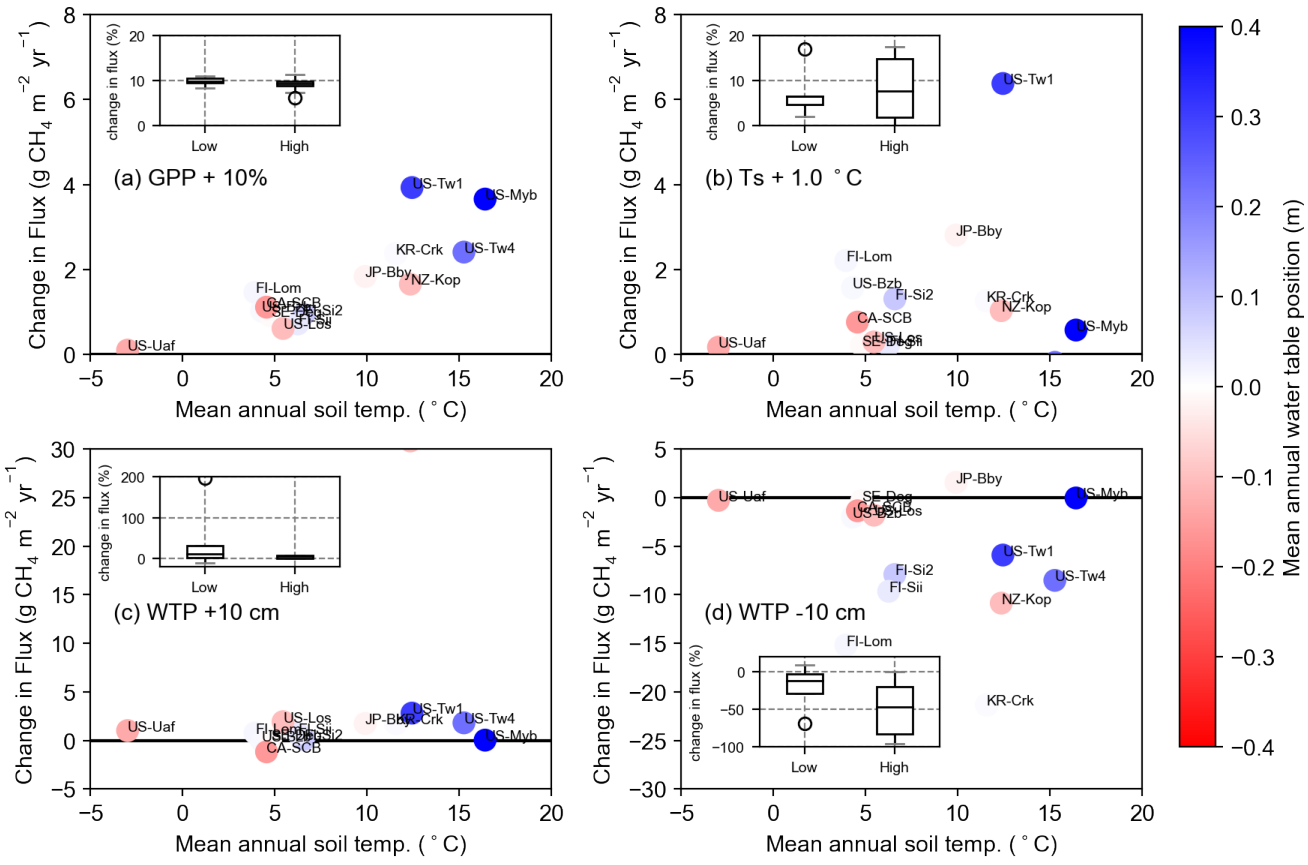

Modeled sensitivity of annual mean methane (CH_4) flux to perturbed input of 10% high gross primary productivity (GPP) (a), biased input of 1°C high soil temperatures (Ts) (b), 10 cm high water table position (WTP) (c), and 10 cm low WTP (d). The changes in fluxes were shown on climate space of mean annual soil temperature and mean annual WTP over the observation period for each site. Boxplots represent the relative changes in flux for aggregated sites having annual high and low mean WTP (higher and lower above the ground, respectively), where dots represent outliers. The relative changes by boxplots did not include US-Uaf, because the flux was too low and the ratio was anomalously high due to low denominator. The sensitivity analysis was done for sites having at least three years of data.

Figure 9

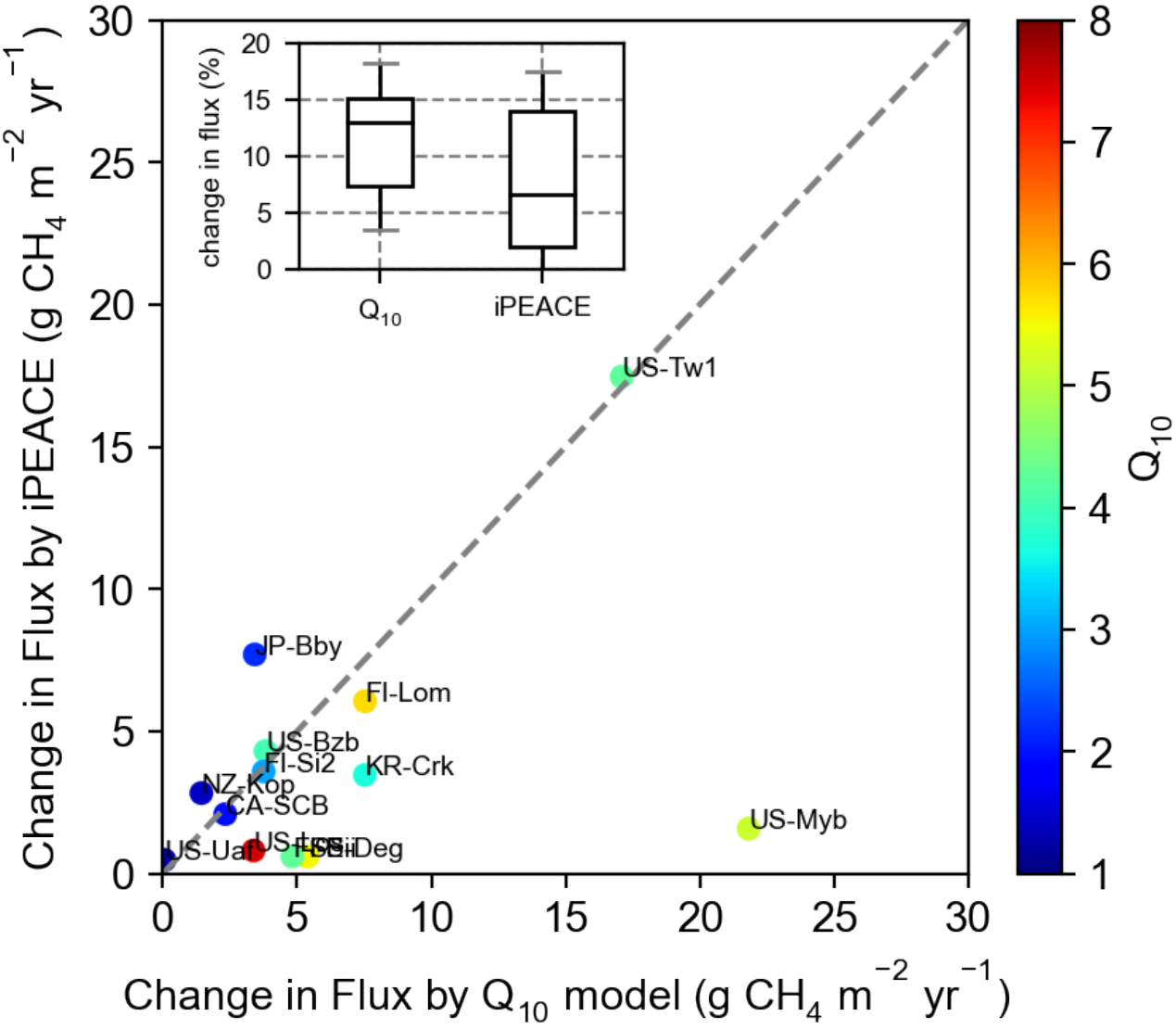

Change in methane (CH_4) flux estimated with a perturbed input of 1°C increase in soil temperatures for the empirical Q_{10} model and iPEACE model. The colors in plots represent the empirical Q_{10} value between daily CH_4 flux and soil temperature for the surface layer. Boxplots represent the relative changes in flux for aggregated sites having annual high and low mean water table positions (higher and lower above the ground, respectively). The relative changes by boxplots did not include US-Uaf, because the flux was too low and the ratio was anomalously high due to low denominator.

Table 1. Literature survey for partitioned mathane (CH_4) emissions from wetlands (i.e., ebullition diffusion, and plant-mediated transport) based on field observations and modeling.

Obs./Model	Wetland Type	Site	Ebullition	Diffusion	Plant	Method	Period	Reference
Observation	Arctic Tundra				92-98	Chamber	Summer	Morrissey and Livingston, 1992
Observation	Arctic Tundra				66 (polygon center) 27 (polygon rim)	Chamber	August	Kutzbach et al., 2004
Observation	Arctic Tundra	RU-Ch2	2		25 (wet sites) 0 (dry sites)	Chamber	Summer	Kwon et al., 2017
Observation	Boreal bog	FI-Si2	2-8		31	Bubble trap Chamber	Growing season	Männistö et al., 2019 Korrensalo et al., 2022
Observation	Boreal fen	FI-Sii			21	Chamber		Korrensalo et al., 2022
Observation	Boreal fen				38 (hummocks) 31 (lawns) 51 (hollows)	^{14}C pulse labeling of mesocosms	12 days	Dorodnikov et al., 2011
Observation	Temperate bog	JP-Bby	50			Chamber	Summer	Tokida et al., 2007a, b
Observation	Temperate bog		14-16			Bubble trap	Growing season	Stamp et al., 2013
Observation	Temperate bog				64-90	Chamber	May-December	Shannon et al., 1996
Observation	Temperate fen		38			Bubble trap	Spring & summer	Stanley et al., 2019
Observation	Temperate fen		~ 10			Eddy covariance for isoflux	two days in summer	Santoni et al., 2012
Observation	Temperate fen (*Eriophorum vaginatum*) Temperate fen (*Sphagnum* spp. & *Betula* spp.)	FR-LGt	54.7 in May 40.7 in March negligible			Chamber Combined eddy covariance and process study	two months	Gogo et al., 2011
Observation	Temperate marsh (open water)	US-Myb	~ 1.3	~ 4.1		Bubble trap in open water area within the flux footprint Gas concentration in water for open water area	Annual	McNicol et al., 2017
Observation	Temperate marsh (open water)		50	50	Not consier	Chamber at water surface not including vegetation		
Observation	Temperate marsh (floating vegetation)		50	50	Not consier	Chamber at water surface not including vegetation	September	Villa et al., 2021
Observation	Temperate marsh (emergent vegetation)		99	1	Not consier	Chamber at water surface not including vegetation		
Observation	Temperate marsh (emergent vegetation)	US-Tw1	10-30			Static chambers	Aug. 29- Sep. 2	Windham-Myers et al. (2018)
Observation	Rice paddy		9			Eddy covariance + Wavelet analysis	Growing season	Richardson et al., 2022
Observation	Rice paddy	KR-Crk	10-17			Eddy covariance + Wavelet analysis	Growing season	Hwang et al., 2020
Observation	Rice paddy			marginal	60-90	Chamber	Growing season	Butterbach-Bahl et al., 1997
Observation	Rice paddy		4	marginal	96	Chamber	Growing season	Kajiura and Tokida, 2021
Model	pan-Arctic wetland (regional mean)		51.5	1	47.5	VISIT	Annual	Ito 2019
Model	Boreal bog		0.6	3.4	96	TECO calibrated with chamber data	Annual	Ma et al., 2017
Model	Boreal fen	FI-Sii	0	37	63	HIMMELI calibrated with eddy covariance data	Annual	Peltola et al., 2018
Model	Boreal fen	FI-Sii	5	30	75-95	sqHIMMELI calibrated with eddy covariance data	Annual	Susiluoto et al., 2018
Model	Arctic Tunder near RU-Ch2		4.2	34.8	61.0	JSBACH-methane	Annual	Castro-Morales et al., 2018
Model	Alpine tundra (Ruoergai)		0.3	28.8	70.8	LPJ-WHyMe v 1.3.1	Annual	Wania et al., 2010
Model	Subarctic mire (Abisko)		0	15.5	84.5	LPJ-WHyMe v 1.3.1	Annual	Wania et al., 2010
Model	Boreal fen (BOREAS)		0.9	29.2	69.9	LPJ-WHyMe v 1.3.1	Annual	Wania et al., 2010
Model	Boreal fen (Salmisuo)		1.4	30.9	67.8	LPJ-WHyMe v 1.3.1	Annual	Wania et al., 2010
Model	Boreal fen (Degero)		0.8	25.7	74.3	LPJ-WHyMe v 1.3.1	Annual	Wania et al., 2010
Model	Temperate bog (Michigan)		0	24.4	75.6	LPJ-WHyMe v 1.3.1	Annual	Wania et al., 2010
Model	Temperate fen (Minnesota)		0.4	22.9	76.7	LPJ-WHyMe v 1.3.1	Annual	Wania et al., 2010
Model	Temperate fen	US-Los	0.0	23.7	76.3	ORCHIDEE-PEAT revision 7020	Annual	Salmon et al., 2022
Model	Boreal bog	US-Bzb	0.0	0.9	99.1	ORCHIDEE-PEAT revision 7020	Annual	Salmon et al., 2022
Model	Temperate fen	FR-LGt	0.0	-0.1	100.1	ORCHIDEE-PEAT revision 7020	Annual	Salmon et al., 2022
Model	Boreal fen	FI-Lom	0.8	-1.6	100.8	ORCHIDEE-PEAT revision 7020	Annual	Salmon et al., 2022
Model	Temperate Marsh	US-Wpt	0.0	0.0	100.0	ORCHIDEE-PEAT revision 7020	Annual	Salmon et al., 2022

Table 2 Description of study sites, showing wetland type, location, dominant vegetation type (DOM_VEG), mean annual air temperature (TAVE), GPP, annual maximum monthly leaf area index (LAI) (MCD15A3H), mean annual soil temperature (TS), water table depth during the period when soil was thaw (WTD gs), and modeled partitioned methane (CH_4) emissions during the growing season when LAI was higher than 20% of the annual maximum.

Site	Wetland type	Latitude	Longitude	DOM _VEG	TAVE (℃)	GPP (g C m^{-2} yr^{-1})	LAI (m^2 m^{-2})	TS (℃)	WTD gs (m)	WTD min (m)	Start year	End year	Ebullition (%)	Plant (%)	Diffusion (%)	References
RU-Ch2	Tundra	68.617	161.351	aerenchymatous	-10.6	284	2.0	-5.0	-0.01	-0.02	2014	2015	50	49	1	Goeckede (2020)
US-Ics	Tundra	68.606	-149.311	aerenchymatous	-5.9	237	1.7	-0.8	-0.01	-0.02	2015	2016	35	65	0	Euskirchen et al. (2020)
SE-Sto	Bog	68.356	19.0452	aerenchymatous	0.7	197	1.4	0.2	0.09	0.09	2014	2015	0	53	47	Knox et al. (2019)
FI-Lom	Fen	67.99724	24.20918	aerenchymatous	-0.4	434	2.0	3.9	0.02	-0.04	2006	2010	23	77	0	Lohila et al. (2020)
US-Uaf	Bog	64.86627	-147.8555	moss_sphagnum	-2.9	599	1.4	-3.0	-0.14	-0.42	2011	2018	18	70	12	Iwata et al. (2020)
US-Bzf	Fen	64.703733	-148.3133	aerenchymatous	-0.2	581	2.3	4.7	0.00	-0.01	2015	2016	--	--	--	Euskirchen and Edgar (2020a)
US-Bzb	Bog	64.695547	-148.3208	eri_shrub	-0.7	570	1.5	4.3	0.02	0.00	2014	2016	68	31	1	Euskirchen and Edgar (2020b)
SE-Deg	Fen	64.182029	19.556539	moss_sphagnum	2.5	241	2.2	4.8	-0.01	-0.29	2014	2018	12	84	5	Nilsson and Peichl (2020)
FI-Si2	Bog	61.837459	24.169896	moss_sphagnum	5.1	275	2.2	6.6	0.09	-0.07	2012	2016	16	67	17	Vesala et al. (2020a)
FI-Sii	Fen	61.832562	24.192933	moss_sphagnum	4.7	319	2.4	6.2	0.03	-0.17	2013	2018	9	91	0	Vesala et al. (2020b)
CA-SCB	Bog	61.308	-121.299	moss_sphagnum	-1.5	312	2.9	4.6	-0.16	-0.37	2014	2017	11	78	11	Sonnentag and Helbig (2020)
DE-Hte	Fen	54.210278	12.17611	aerenchymatous	10.0	774	4.9	10.6	-0.27	-0.62	2011	2018	--	--	--	Koebsch and Jurasinki (2020)
DE-Zrk	Fen	53.8759	12.88901	aerenchymatous	9.5	598	2.8	10.9	0.23	-0.12	2013	2018	--	--	--	Sachs and Wille (2020)
DE-Sfn	Bog	47.806389	11.3275	tree	8.3	772	2.9	7.8	-0.07	-0.24	2012	2014	--	--	--	Schmid and Klatt (2020)
FR-LGt	Fen	47.32291	2.284102	aerenchymatous	11.0	952	4.6	10.5	-0.23	-0.46	2017	2018	12	87	1	Jacotot et al. (2020)
US-Los	Fen	46.0827	-89.9792	eri_shrub	4.9	712	6.5	5.4	-0.11	-0.45	2014	2018	9	91	0	Desai (2020)
JP-Bby	Bog	43.323006	141.8107	aerenchymatous	7.0	737	2.7	9.9	-0.02	-0.23	2015	2018	27	70	2	Ueyama et al. (2020)
US-Wpt	Marsh	41.464639	-82.99616	aerenchymatous	11.3	636	2.8	13.4	0.38	0.14	2011	2013	--	--	--	Chen and Chu (2020)
KR-Crk	Rice	38.2013	127.2506	aerenchymatous	10.9	975	2.0	11.5	0.01	0.00	2015	2018	61	39	0	Ryu et al. (2020)
US-Tw1	Marsh	38.107	-121.647	aerenchymatous	15.1	1617	1.7	12.4	0.30	-0.48	2011	2018	26	45	29	Valach et al. (2020b)
US-Tw4	Marsh	38.103	-121.641	aerenchymatous	15.5	1048	1.3	15.3	0.23	-0.37	2013	2018	42	57	0	Eichelmann et al. (2020)
US-Myb	Marsh	38.05	-121.765	aerenchymatous	15.5	1157	2.1	16.4	1.23	0.68	2010	2018	18	58	24	Matthes et al. (2020)
US-Sne	Marsh	38.037	-121.755	aerenchymatous	15.0	329	1.8	16.9	0.10	-0.58	2016	2018	--	--	--	Shortt et al. (2020)
JP-Mse	Rice	36.054	140.0269	aerenchymatous	13.7	960	2.1	14.5	-0.01	-0.03	2012	2012	12	65	23	Iwata (2020)
NZ-Kop	Bog	-37.388	175.554	aerenchymatous	13.7	1017	5.0	12.4	-0.10	-0.29	2012	2015	30	70	0	Campbell and Goodrich (2020)

Table 3. Ranges of parameters for mathematical optimization and prior distributions for Bayesian optimization for the iPEACE model. The range of uniform distributions were determined by adding plus/minus to the values determined by the differential evolution method for each site (Table S1)

Parameter	Unit	Lower range in mathematical optimization	Upper range in mathematical optimization	Prior range in Bayesian inference	Prior distribution
Initial CH_4 value at the surface layer	mol-CH_4 m^{-3}	0	0.5	±0.1	uniform
Initial CH_4 value at the deep layer	mol-CH_4 m^{-3}	0	4	±0.2	uniform
Base production rate per gross primary productivity ($p_{production}$)	mmol-CH_4 g C^{-1}	1	6	±0.5	uniform
Temperature sensitivity of CH_4 production ($Q_{10producton}$)	--	0.00001	5	±1	uniform
Maximum CH_4 oxidation rate ($p_{oxidation}$)	mol-CH_4 m^{-2} s^{-1}	0.000000125	0.000125	±log(1.0)	uniform
Nondimensional conductivity for gaseous transfer ($p_{ebullition}$)	--	0	0.01	b	uniform
Diffusion coefficient for plant-mediated transport (p_{plant})	10^{-3} d^{-1}	0.001	3	±1	uniform
Diffusion coefficient multiplier for water ($p_{diffusion-water}$)	--	0.001	2	±0.3	uniform
Diffusion coefficient multiplier for gas ($p_{diffusion-gas}$)	--	0.001	2	±0.3	uniform
Sensitivity of ebullition to barometric pressure ($p_{pressure}$)	hPa^{-1}	0	1	±0.05	uniform
Thickness of the surface layer (z_{surf})	m	0.05	0.80	0.05-0.80	uniform
Surface root fraction (fs_{root})	--	0.05	1.00	0.05-1.00	uniform
Residuals of the model	mg CH_4 m^{-2} d^{-1}	--	--	--	log normal